Energy levels of Pr^{3+} in $Y(OH)_3$ determined from absorption and fluorescence spectra
by James Keith Boger

A thesis submitted in partial fulfillment of the requirements for the degree of Master of Science in Physics
Montana State University

Abstract:
In this thesis, the electronic energy levels in the 4f subshell of a trivalent lanthanide in an optically transparent crystal are found. The particular crystal studied was trivalent praseodymium in yttrium hydroxide. Determination of the levels was accomplished by comparing experimentally found energies to the eigenvalues of a Hamiltonian whose form had been given. Experimental energies were found by studying emission and absorption spectra from the sample. This thesis begins by outlining the theory behind the project. Details of the experimental arrangement, data analysis and results from the calculations are then presented. As final results, the calculated energy levels as well as their experimental counterparts are presented. Also presented are the magnitudes found for the parameters in the Hamiltonian of the sample.

ENERGY LEVELS OF Pr^{3+} IN $Y(OH)_3$ DETERMINED FROM ABSORPTION AND FLUORESCENCE SPECTRA

by

James Keith Boger

A thesis submitted in partial fulfillment
of the requirements for the degree

of

Master of Science

in

Physics

MONTANA STATE UNIVERSITY
Bozeman, Montana

July 1987

APPROVAL

of a thesis submitted by

James Keith Boger

This thesis has been read by each member of the thesis committee and has been found to be satisfactory regarding content, English usage, format, citations, bibliographic style, and consistency, and is ready for submission to the College of Graduate Studies.

July 27, 1987 — Rufus L Cone

Date — Chairperson, Graduate Committee

Approved for the Major Department

7/27/87 — D J Swenson

Date — Head, Major Department

Approved for the College of Graduate Studies

8-25-87 — M Malone

Date — Graduate Dean

STATEMENT OF PERMISSION TO USE

In presenting this thesis in partial fulfillment of the requirements for a master's degree at Montana State University, I agree that the Library shall make it available to borrowers under the rules of the Library. Brief quotations from this thesis are allowable without special permission, provided that accurate acknowledgment of source is made.

Permission for extensive quotation from or reproduction of this thesis may be granted by my major professor, or in his absence, by the Dean of Libraries when, in the opinion of either, the proposed use of the material is for scholarly purposes. Any copying or use of the material in this thesis for financial gain shall not be allowed without my written permission.

Signature James K. Boyer

Date August 3, 1987

TABLE OF CONTENTS

LIST OF TABLES

LIST OF FIGURES

LIST OF FIGURES-continued

ABSTRACT

In this thesis, the electronic energy levels in the 4f subshell of a trivalent lanthanide in an optically transparent crystal are found. The particular crystal studied was trivalent praseodymium in yttrium hydroxide. Determination of the levels was accomplished by comparing experimentally found energies to the eigenvalues of a Hamiltonian whose form had been given. Experimental energies were found by studying emission and absorption spectra from the sample. This thesis begins by outlining the theory behind the project. Details of the experimental arrangement, data analysis and results from the calculations are then presented. As final results, the calculated energy levels as well as their experimental counterparts are presented. Also presented are the magnitudes found for the parameters in the Hamiltonian of the sample.

CHAPTER 1

INTRODUCTION

This thesis concentrated on the emission and absorption spectra of a trivalent lanthanide in a host lattice. In general one might ask what is special about trivalent lanthanides. From a scientific point of view these elements are interesting because they have many extremely narrow emission and absorption linewidths in the visible spectrum.[1] Furthermore, trivalent lanthanides can be incorporated into various optically transparent materials. This is convenient due to the fact that the oscillator strengths, or transition probabilities, of the free ions are very small, while they can be significant when the ion is trapped in a host lattice. Large oscillator strengths suggest that a large number of lanthanide ions may be optically pumped into an excited state. These properties lead to the practical applications of trivalent lanthanides in host lattices as laser materials. The YAG laser, with trivalent neodymium, is a graphic example of the practical role these materials have.

Typically, before any applications for a material can be envisioned, it is necessary to establish some fundamental properties of that material. For optically transparent glasses and crystals doped with a trivalent rare earth, the energy levels are among the first bits of information established. Finding the energy levels of trivalent praseodymium in a crystal of yttrium hydroxide, $Pr^{3+}:Y(OH)_3$, was the motivation for this thesis. This information could then be used in carrying out further experiments on the sample such as optical hole burning.[2]

A brief outline of the procedure used in seeking the energy levels of the sample is facilitated by following the flow chart given in Figure 1. The first box in this flow chart labeled 'Experiment', indicates that the first step in the project was to experimentally observe as many transitions in the sample as possible. As indicated, recording absorption and fluorescence transitions made up the two types of experiments conducted. Of course just because many spectral lines may be recorded, does not mean that the states involved in each transition are known. It is therefore necessary to develop a method for analyzing the data. The second box entitled 'Data Analysis', indicates a general outline of the scheme designed to interpret the data. In general, the method used was to make a list of all possible transitions which might be responsible for each spectral line recorded. Then by making a choice from each list, a set of experimentally

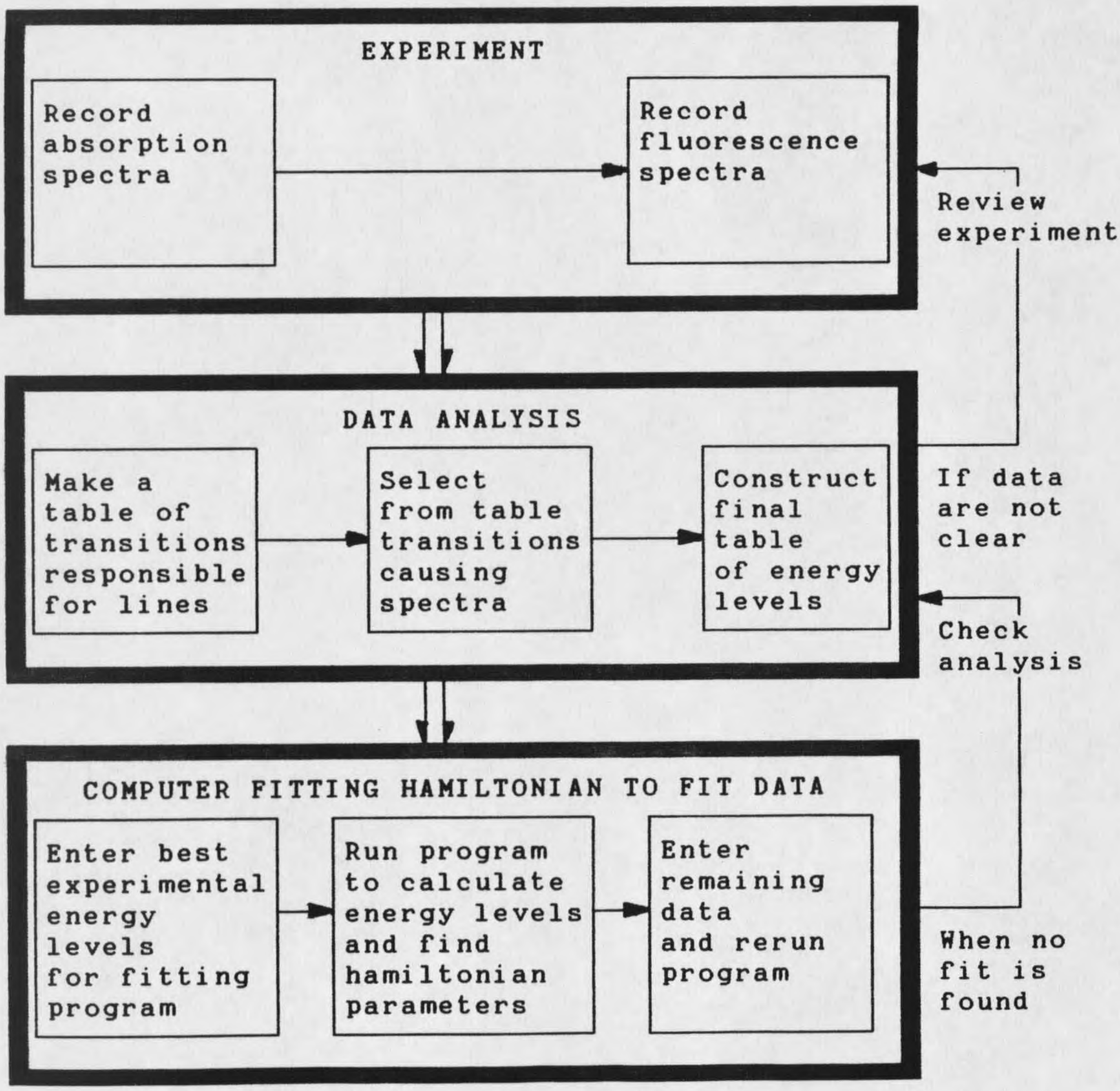

Figure 1. Thesis outline

determined energy levels could be constructed. But it was impossible to experimentally determine every energy level in the sample, so it was necessary to turn to theoretical aspects of the energy levels.

Theoretically, all of the energy levels could be calculated if the Hamiltonian of the sample was known. While the form of the Hamiltonian is known, the magnitudes of the various parameters are not. It is therefore necessary to take the energy levels determined experimentally to empirically determine the magnitude of these parameters. This was done by entering the experimental data into a computer program which modeled the Hamiltonian by solving the eigenvalue problem and then comparing the results to the entered data. If a Hamiltonian is found having eigenvalues which are close to the experimental values, then all of the energy levels can be considered known. The typical situation however was to find contradictions between experimental and calculated values. Contradictions made it necessary to check the selections made during the data analysis step. These selections often proved to be ambiguous, forcing the experiment itself to be repeated.

This thesis reports on the method used in seeking the energy levels of $Pr^{3+}:Y(OH)_3$ and the results obtained. The discussion begins in Chapter 2 with the fundamental theoretical ideas necessary to understand the goals of this work. After investigating some theoretical aspects, the discussion closely follows the flow chart in Figure 1, explaining each section in considerable detail. So, Chapter 3 explains the experimental arrangement and procedure used in recording spectra from the sample. Chapter 4 investigates the exact procedure used to analyze the data from the experiments. Chapter 5 is then a discussion of the method and tools used to find the correct Hamiltonian and thereby the correct energy levels for $Pr^{3+}:Y(OH)_3$. Finally Chapter 6 presents the results obtained and conclusions made from this work.

CHAPTER 2

THEORY

The main thrust of this thesis concerned recording and studying spectra. It is therefore natural to begin the discussion of the theory behind the project by explaining some fundamentals of spectroscopy. Attention is then directed towards the specific sample studied. The sample which this project focused on was trivalent praseodymium in a crystal of yttrium hydroxide ($Pr^{3+}:Y(OH)_3$). There are several aspects of the sample which should be understood before studying the experimental spectra. Specifically we need to know what possible energy levels to expect and what the selection rules are. After studying the spectrum, the data are used to construct a Hamiltonian, which when diagonalized should yield the energy eigenvalues. Before any modeling can be done, the full form of the Hamiltonian needs to be introduced. To accomplish this, the discussion is broken into two parts: the free ion Hamiltonian and the crystal field Hamiltonian.

Spectroscopy

Spectroscopy concerns scanning the electromagnetic spectrum for signals emitted or absorbed by the sample being studied. Generally frequency is used to index the spectrum but here wavenumbers, which have units of cm^{-1}, are used. The relationship between wavenumbers and the energy states of the electron is simply given by the Bohr postulate for radiating atoms.

$$\frac{c(E_f - E_i)}{h} = \frac{1}{\lambda} \qquad 1$$

Here E_f and E_i refer to the initial and final energies respectively and λ is used for wavelength. One may ask at this point what good this equation does since there are two unknowns in energy. It is in determining these energies that spectroscopy finds its greatest use. The experimental section specifically addresses this question. For now let it suffice to say that by obtaining many spectral lines one can logically deduce what the initial and final states are. The catalyst for this deduction lies in finding spectral absorption first where the initial energy can be assumed to be zero.

Bohr's postulate for the wavenumber of the photon is simply a statement of energy conservation. It is interesting to investigate the origins of this electromagnetic radiation because it gives some insight into the quantum mechanics of the atom. The most efficient source of electromagnetic radiation is the electric dipole oscillator. The power which is radiated by such an oscillator is given by[3]

$$P = \frac{ck^4}{3}\,|d|^2 \qquad 2$$

Here d is the dipole moment and k is the magnitude of the wavevector. From this it can be seen that the link between radiated electromagnetic energy and the states of the atom lies in the nonzero value for the dipole moment.

To establish this link it is helpful to calculate the electric dipole moment starting with the time dependent quantum states of the atom. The strength of a dipole is given as

$$d = e|\langle i|\mathbf{r}|f\rangle|. \qquad 3$$

In this expression, $\langle i|\mathbf{r}|f\rangle$ refers to the expectation value for the electron's position when it is between initial and final states and e is its charge. To calculate the expectation value it is necessary to know the state of the atom. In a one electron atom the state may be expressed in ket form as $|nlsjm_j\rangle$. During the time that the electron is making a transition from one state to another, it can be thought of as being in a superposition of the states involved. Upon calculating the expectation value an oscillation in time is found as shown by

$$\langle i|r|f\rangle \quad \cos(wt). \qquad (4)$$

Here w is the angular frequency $(E_i - E_f)/h$, and translates as the angular frequency of the emitted photon. The oscillating expectation value means the dipole is oscillating and therefore P in equation 2 is nonzero, proving the atom radiates.

Figure 2 is a graphical representation of the oscillating dipole using the harmonic oscillator as a model. The first two graphs in Figure 1 represent the wave functions of the ground and first excited state of the harmonic oscillator. The third graph represents the superposition state that the electron must be in during the transition. If the superposition state is squared, the probability distribution of the electron is obtained as shown in the fourth graph. This asymmetric distribution clearly shows the nonzero dipole. Following the time evolution of the states shows that this dipole is oscillating as suggested by the double headed arrow over the fourth plot and by equation 4. The careful reader may have also noticed that the states involved in the transition were of different parity.[4] This is a requirement for a nonzero dipole moment and leads to the fact that the quantum numbers involved are not completely arbitrary.

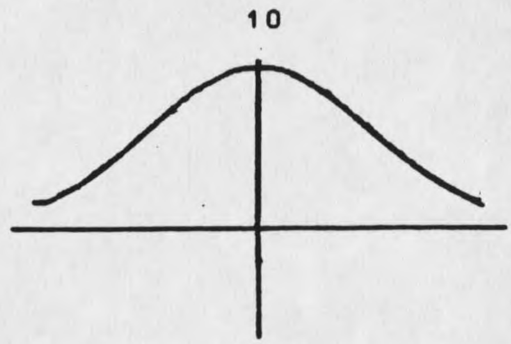

(a) Ground State

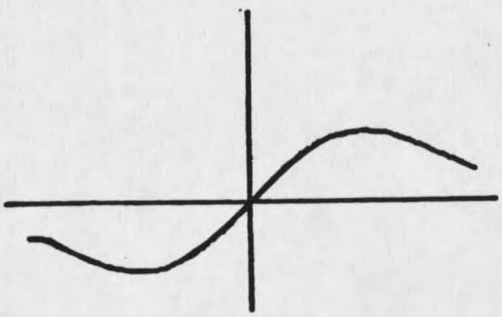

(b) First excited state

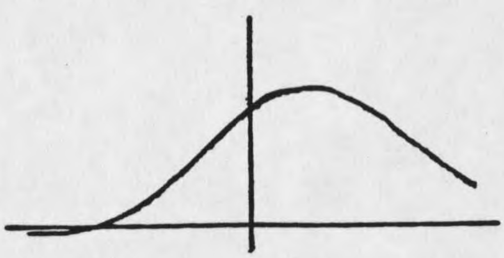

(c) Superposition of states

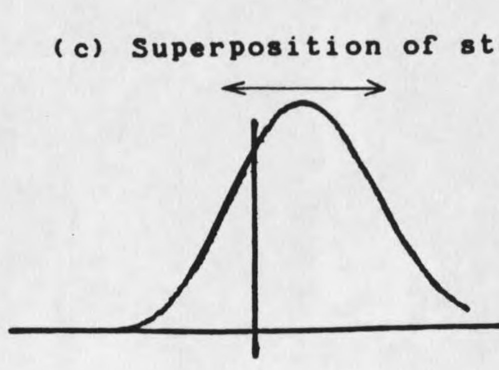

(d) Probability distribution

Figure 2. Plots of the harmonic oscillator.

The restrictions placed on the quantum numbers are referred to as the selection rules. For a one electron atom emitting electric dipole radiation the selection rules are as follows:

Δn unrestricted
$\Delta l = \pm 1$
$\Delta j = \pm 1, 0$
$\Delta m_j = \pm 1, 0$

These selection rules may be found in any book on quantum mechanics such as Liboff.[5] Of course there can be violations of these rules resulting from transitions which are not dipole in nature. Electric quadrupole radiation is a good example of this. However, the intensity of a nondipole transition is very weak and could safely be ignored in this project. If the quadrupole moment were large enough to worry about, a new set of selection rules would have to be introduced.

While the transitions studied in this project were dipole in nature, the one electron selection rules turned out to be invalid. The most blatant violation occurs when we consider that all of the transitions studied occurred within the 4f subshell suggesting Δl equal to zero. The seemingly forbidden transitions occur because the crystal field interacts with the free ion, mixing states of different parity with the 4f states and thereby allowing the transitions.[6] When considering the sample in more detail, new pertinent selection rules are presented. These selection rules turn out to be important when determining energy levels.

Praseodymium as a Free Ion

Praseodymium is a rare earth element in the lanthanide series. Like all other lanthanides, praseodymium has an unfilled 4f subshell which is spatially located within the 5s, 5p and 6s subshells. This results in the valence electrons being shielded from outside perturbations which in turn gives rise to sharp spectral lines, even when the atoms are fixed in a host lattice. Another interesting property of the lanthanides is the fact that there are many visible spectral lines resulting from transitions within the 4f subshell.

The electronic configuration of the praseodymium atom is given by

$[Xe]\ 4f^3 6s^2$.

The atom which was studied was triply ionized. Because xenon is a noble element with a relatively high ionization energy, the three electrons will be removed from the 4f and 6s subshells. The electronic configuration of Pr^{3+} is then given by

$[Xe]\ 4f^2$.

Typically, the states of the system are expressed in spectroscopic notation. In this notation, the sum of the l s and j quantum numbers for all of the electrons in the valence subshell are specified. In the case of Pr^{3+} there are two contributing electrons, each having a maximum orbital angular momentum of 3. This gives rise to the following possible terms for total orbital angular momentum:

$$\begin{array}{ccccccccc} & & S & P & D & F & G & H & I \\ L & = & 0 & 1 & 2 & 3 & 4 & 5 & 6. \end{array}$$

Additionally each electron has a spin angular momentum of one half, suggesting that each term given above may be either singlet or triplet. The next goal is to determine what order these terms must be in.

In finding what order the term notation must be in, it is only natural to begin with finding the ground state. This is easily accomplished by applying Hund's rules. Doing this, it is found that the ground state of Pr^{3+} is given in term notation as $^3H_4$.

To find the ordering of all other terms, it is necessary in principal to diagonalize the appropriate Hamiltonian. The Hamiltonian for the lanthanide series of free ions has been worked out by several workers such as Judd, Dieke and Wybourne. The reader may find a full accounting of the free ion theory in Wybourne's book.[7] Most of the discussion on the Hamiltonian presented here is based on an excellent review of the subject by Hüfner.[6]

The only atomic Hamiltonian for which the Schrödinger equation may be solved exactly is that for the hydrogen atom. This means that for the Pr^{3+} ion, perturbation theory must be used. This theory allows us to split the Hamiltonian, as in equation 5, into a unperturbed term representing the hydrogenic system and a perturbed term representing complicating factors such as electron-electron interactions.

$$H = H_{HS} + H_P \tag{5}$$

The idea behind perturbation theory is to solve the Schrödinger equation with the unperturbed Hamiltonian first and thereby obtain a set of basis states. With these states, a matrix of the perturbation term may be constructed and diagonalized for energies. The energy of the system may then be expressed by

$$E = E_{HS} + E_P. \tag{6}$$

So it is seen that calculating the perturbation energies E_P is the primary goal since the energy derived from the hydrogenic term E_{HS}, simply adds a constant to the total energies. With the ideas of perturbation theory in hand, it is possible to focus on the pertinent Hamiltonian for Pr^{3+}.

In light of perturbation theory, it is clear that only perturbation terms to a central field Hamiltonian need be considered. For trivalent praseodymium the perturbation Hamiltonian has been given by W. T. Carnall et al.[8] as

$$H_f = \Sigma F^k f_k + \zeta A_{so} + \alpha L(L+1) + \beta G(G_2) + \gamma F(R_2) + \Sigma M^k m_k + \Sigma P^k p_k. \qquad 7$$

The first term in this expression represents the coulomb interaction between the two electrons with F^k being an adjustable parameter. The second term considers the spin orbit interaction between the electron and the nucleus. The adjustable parameter for spin orbit is ζ. Spin orbit corrections appear even for one electron systems, so it is not surprising that two electron systems have additional spin orbit corrections. These additional corrections are accounted for by the P^k parameters.(9) The M^k parameters account for relatively small effects of spin-spin interactions and spin-other-orbit interaction. These interactions are between the two valence electrons.(6) Finally, the α, β and γ parameters consider corrections due to higher configuration interactions.(10)

At this point, if the magnitude of each parameter were known, then the energy eigenvalues could be calculated. However, Pr^{3+} is usually studied in a crystal or a glass. The exception to this was work done by J. Sugar studying the spectra of Pr^{3+} in the vapor state.(11) Using Sugar's values, and studying the values obtained from the spectra of $Pr^{3+}:LaCl_3$ and $Pr^{3+}:LaF_3$,(8) an estimation of the free ion energy levels was made. The estimated levels appear in Figure 3.

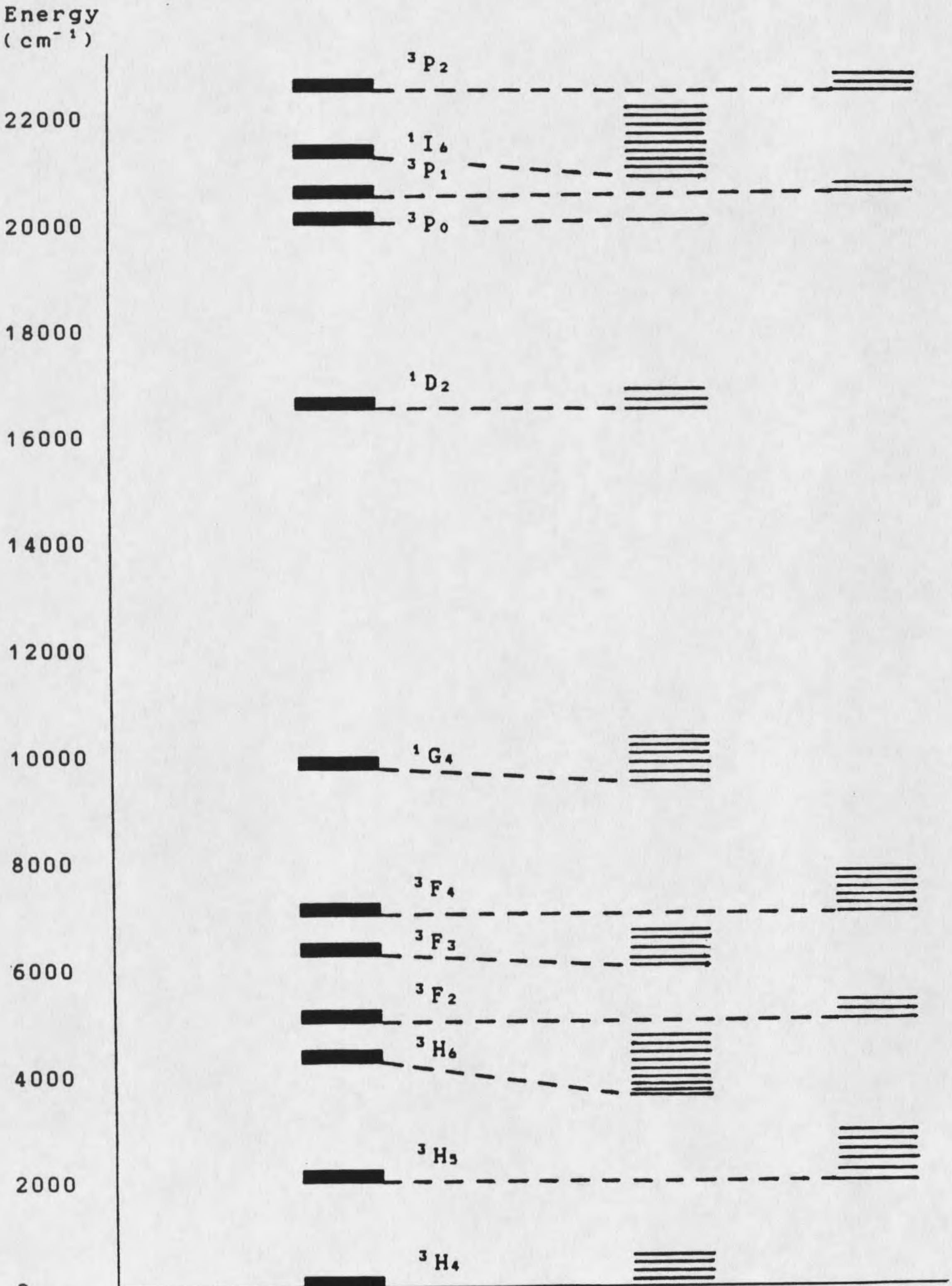

Figure 3. Estimated energy levels for Pr^{3+}: $Y(OH)_3$.

Praseodymium in a Crystal Field

When the Pr^{3+} ion is in a crystal field, some of the 2j+1 degeneracy of the free ion is partially removed. This is due to the fact that adding the crystal field to the Hamiltonian removes the spherical symmetry from the ion's environment. Naturally it is necessary to know what the possible states are before studying the experimental spectra. To determine the these states, it is necessary to know the form of the crystal field part of the Hamiltonian. To facilitate the explanation of finding the states, it is convenient to consider the crystal field part of the Hamiltonian alone. By doing this, we are effectively diagonalizing a submatrix of the Hamiltonian. This section concludes with the selection rules pertinent for $Pr^{3+}:Y(OH)_3$.

The crystal field results from the praseodymium ion occupying a site in the crystal lattice normally occupied by a yttrium atom. The sample studied was $Y(OH)_3$ doped with 1% Pr^{3+}. This means that the crystal was grown from a solution such that 1% of the yttrium atoms were replaced with Pr^{3+} ions. The crystal field is then produced primarily by the $(OH)_3$ molecules which surround each Pr^{3+} ion. The potential can be expressed in terms of a series of spherical harmonics. This means that the crystal field

Hamiltonian can be expressed by

$$H_{cf} = \Sigma_{lm} B^{l}_{m} C^{l}_{m}. \qquad 8$$

Here the B's are parameters while the C^{l}_{m} represent renormalized spherical harmonics. The Y's and C's are related by

$$C^{l}_{m} = \frac{4\pi}{(2m+1)} Y^{l}_{m}. \qquad 9$$

The reader may find a good explanation of crystal field expressions in Weissbluth's book.[12] So at this point, H_{cf} is expressed in an infinite series in the orbital angular momentum sum which must be truncated. The triangle relation for angular momenta immediately limits the series to values less than 2l.[12] For two f electrons this means that the sum can only run as high as six. Also, the Pr^{3+} ion occupies a point in the lattice with a relatively high symmetry and this allows us to further limit the series representing the crystal field Hamiltonian.

The point group symmetry for the Pr^{3+} ions is C_{3h}. In the language of group theory, C_3 means that identical properties are found in the crystal for each rotation of $(2/3)\pi$ in a plane perpendicular to the crystal axis. The h in this notation refers to the fact that identical properties are found upon a reflection through the horizontal plane. Figure 5 on page 26 is a drawing of the crystal with the axis shown. By definition of a symmetry operator, it must commute with the Hamiltonian. The free ion Hamiltonian is spherically symmetric, so it is necessary only to consider the crystal field Hamiltonian. In other words, any terms in the expansion in spherical harmonics which do not commute with the C_{3h} operator must have coefficients of zero. This leads to the crystal field Hamiltonian given by Carnall et al.[8]

$$H_{cf} = B^2{}_0 C^2{}_0 + B^4{}_0 C^4{}_0 + B^6{}_0 C^6{}_0 + B^6{}_6 [C^6{}_6 + C^6{}_{-6}] \qquad 10$$

Combining equation 10 with equation 7 gives us the total perturbation Hamiltonian for $Pr^{3+}:Y(OH)_3$. There are a total of 18 parameters which must be determined in order to calculate all of the energy eigenvalues. To find values for the parameters, we compared calculated energies to experimental energies. Chapter 5 explores the method for determining the values of these parameters in more detail.

No comparison between calculated and experimental energies can occur until we have experimentally determined several levels. The methods for determining the levels for the experiment are discussed in the data analysis section. Here it is only important to note that determination of the levels is dependent on knowing exactly what levels exist and what selection rules govern dipole transitions. The number of levels is easily obtained by examining the matrix elements of the crystal field Hamiltonian while the selection rules can be obtained by knowing the point group symmetry of the Pr^{3+} ion.

Finding the new states is accomplished by diagonalizing the submatrices which are constructed from each of the 2j+1 degenerate free ion states and H_{cf}. The basis states used are those for the hydrogenic atom and are given in the uncoupled representation as

$$|LSJM_J\rangle = \Sigma\ a(m_l, m_s)\ Y^m{}_l\,|sm_s\rangle. \qquad 11$$

Here the $a(m_l, m_s)$ represent the Clebsch-Gordan coefficients. Recall that the crystal field Hamiltonian is constructed from a set of renormalized spherical harmonics. Because of this, a general outline of the matrix element calculation can be presented by examining the results from one term. However, each element in the matrix is a sum over all terms in H_{cf}. Each term in the matrix is calculated using the inner product.

$$\langle l's'j'm'_J|LM_l|lsjm_J\rangle \qquad 12$$

Because we seek to find out how the m_J degeneracy is removed from each term in the free ion, it is immediately possible to set l, s and j equal to their primed counterparts. Writing out the inner product in terms of equation 11 results in expression 13.

$$\int \Sigma\ a^*(m'_l, m'_s)\,Y^{m'}{}_l\langle sm'_s|\tau Y^M{}_L\ \Sigma\ a(m^l, m_s)\,Y^m{}_l\,|sm_s\rangle\ d\Omega \quad 13$$

The τ which appears before the spherical harmonic is a constant relating the Y's to the C's and also includes the B parameter. This expression at first appears somewhat confusing, so it is helpful to note that the Y^M_L's from the crystal field Hamiltonian depend only on spatial variables The kets representing spin exist in spin space and are therefore unaffected by the Hamiltonian. This fact allows us to combine the spin variables and thereby obtain a relation between m'_s and m_s.

$$\langle sm'_s | sm_s \rangle = \delta_{m_s m'_s} \qquad 14$$

This simply dictates that for a nonzero element, m'_s and m_s must be equal.

Rewriting equation 13, it is clear that the basic mathematical problem lies in evaluating the integral containing the product of three spherical harmonics.

$$\Sigma\ \Sigma\ \Sigma \int \tau a^* a\ (Y^{m'}{}_l)^*\ Y^M{}_L\ Y^m{}_l\ d\Omega \qquad 15$$

Evaluation of this integral is easily accomplished simply by using the Gaunt formula. The primary objective in evaluating the inner product is to determine which elements in the matrix are nonzero. Therefore the following property derived from the Gaunt formula is important.[12]

$$-m'_l + M + m_l = 0 \qquad 16$$

Using this condition and noting the values of M from H_{cf}, we can immediately see a relationship between the orbital azimuthal quantum numbers.

$$m_l = \pm 6,\ 0 \qquad 17$$

This information immediately allows us to construct matrices from which it is possible to determine what states are non-degenerate.

The next problem which must be addressed at this time concerns labeling the states. To explain the labeling of the new set of non-degenerate states, it is helpful to construct the submatrix for the $^3F_3$ term as an example. Figure 4 shows the nonzero elements in the submatrix for the $^3F_3$ term using the conditions given in 17. The dark outlines in Figure 4 suggest that the matrix can be thought of as two submatrices. The upper submatrix is a two by two which diagonalizes to give two states. The lower submatrix, being diagonal, appears to give five possible states. However, due to Kramer's degeneracy (time reversal degeneracy) the state differing only by a sign in the m_l's are still degenerate. The labeling of these states is accomplished with a scheme given by Hellwege and discussed in Hüfner's book.[6] For C_{3h} this scheme defines a new quantum number, μ, which is defined by

$$\mu = m_J (\mathrm{mod}\ 6). \qquad 18$$

The states resulting from the $^3F_3$ term are listed in Table 1. Notice that the states from the two by two matrices are

m'_J \ m_J =	3	-3	2	1	0	-1	-2
3	X	X					
-3	X	X					
2			X				
1				X			
0					X		
-1						X	
-2							X

Figure 4. $^3F_3$ submatrix for the crystal field Hamiltonian. Nonzero elements are indicated.

labeled with the same μ quantum numbers. The two states are clearly different so a prime is used to distinguish between them.

$^3F_3(0)$,	$\mu = 0$	state
$^3F_3(1)$,	$\mu = 1$	state
$^3F_3(2)$,	$\mu = 2$	state
$^3F_3(3)$,	$\mu = 3$	state
$^3F_3(3')$,	$\mu = 3'$	state

Table 1. States of the $^3F_3$ term.

Figure 3 lists all of the possible states in $Pr^{3+}:Y(OH)_3$. Energy level positioning on this Figure is estimated by comparing the energy levels determined for $Pr^{3+}:LaCl_3$, established by Sarup and Crozier.[13]

The last theoretical consideration which must be explored before analyzing the experiment concerns the possible transitions an electron can make. There are two basic transitions which may occur in a crystal: radiative and nonradiative.

Nonradiative transitions may occur via crystal lattice phonons. If phonons are easily able to carry the energy away from the excited ion, then nonradiative transitions are possible. This event becomes more probable when it takes one or two phonons to carry away the energy. In $Y(OH)_3$, phonons exist with energies corresponding to wavenumbers on the order of 3600 cm^{-1} and 900 cm^{-1}.[2] With phonons in this energy range, it is relatively easy to have nonradiative relaxations occur. A good example of this type of transition occurs between the $^3P_0$ and $^1D_2$ states in $Pr^{3+}:Y(OH)_3$. This transition readily occurs because the energy separation between these states is on the order of 3600 cm^{-1} as seen by inspection of Figure 3.

Radiative transitions are primarily electric dipole in nature. These transitions are governed by selection rules which are given in Table 2. In this table π and σ represent the two possible polarizations the emitted or absorbed photon may have. If the photon has a π polarization, then its polarization vector is parallel to the crystal axis. Naturally, σ polarization is perpendicular to the crystal axis. This is graphically represented in Figure 5.

This completes the discussion of the basic theoretical aspects of the project. The ideas presented here help make the experimental arrangement and analysis more plausible.

u =	0	-1	1	-2	2	3
0	--	--	--	σ	σ	π
-1	--	--	σ	--	π	σ
1	--	σ	--	π	--	σ
-2	σ	--	π	--	σ	--
2	σ	π	--	σ	--	--
3	π	σ	σ	--	--	--

Table 2. Selection rules for a crystal having C_{3h} symmetry.

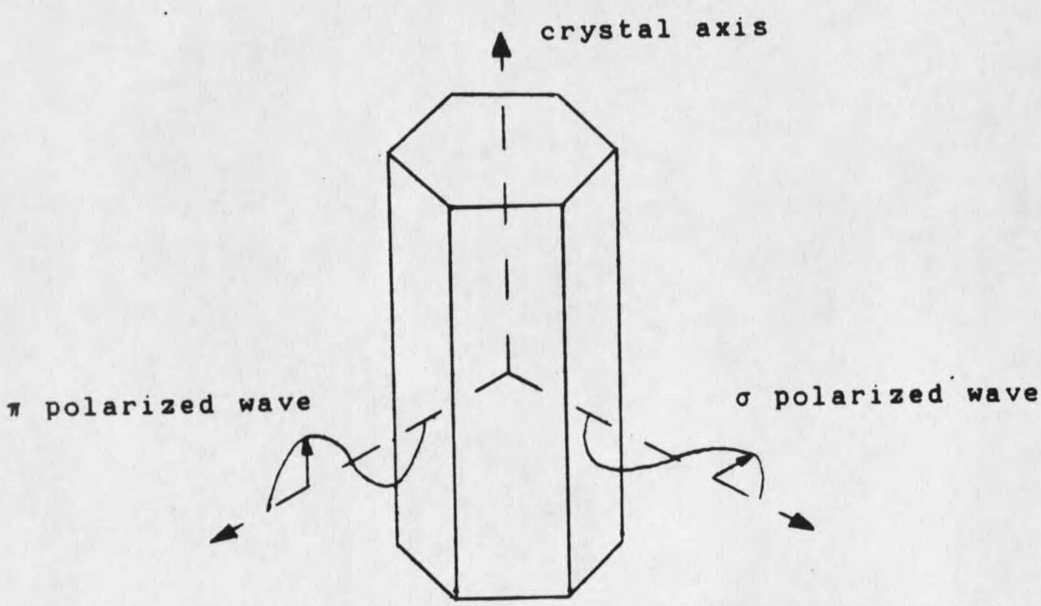

Figure 5. $Pr^{3+}:Y(OH)_3$ sample and relevant polarization.

CHAPTER 3

EXPERIMENTAL ARRANGEMENT

To experimentally determine the energy levels of $Pr^{3+}:Y(OH)_3$, it was necessary to study absorption and fluorescence spectra. Many of the experimental arrangement details in the absorption and fluorescence experiments were similar. This section takes advantage of these similarities by describing one experiment in full and referring back to the details during the explanation of the second experiment. The absorption experiment was the first and the easiest experiment. Therefore this section will begin with a full description of the absorption experiment followed by a description of the fluorescence experiment.

Absorption Experiment

One way of finding the transitions of the electron is by studying the absorption spectrum. This was accomplished by passing white light through the crystal and observing the resulting spectrum. White light of course has a continuous spectrum so the recording instruments simply indicate that they receive a signal for all wavenumbers. Since the white light passes through the crystal, it is possible for some parts of the spectrum to be absorbed. This absorption shows up as a dip in the otherwise continuous spectrum. (See absorption plots in the Appendix). Absorption occurs when the energy of the incident light exactly matches the difference in energy between two states of the ion. It should be noted that the transitions seen may not necessarily be from electrons originating in the ground state of the ion. Instead the electron may be starting from a state with slightly higher energy than the ground state. This results from the thermal excitation in the crystal.

Recall that Boltzman's result tells us the probability that an ion will be in the excited state.

$$P(E) = P(0)e^{-(E/kT)} \qquad 19$$

Here E is used for energy and k is Boltzman's constant. To insure that most of the ions are in the ground state, it is sufficient to require that the probability of being in a state with energy E be at or below $P(0)e^{-1}$. This suggests that $kT = E$. Plugging into this relation in terms of wavenumbers gives a value of about $1.44K/cm^{-1}$. Assuming the first state above the ground state has an energy corresponding to $10cm^{-1}$ or more, then the crystal would have to be at a temperature of at least 14K. This assumption was based on studies of the energy levels of trivalent praseodymium in other crystals.[13,14] The relatively high temperature suggests that a crystal submerged in liquid helium (T < 4K) would insure that all of the electrons would be in the ground state. With the crystal at these very low temperatures, it was possible to determine the energy levels directly from the absorption lines recorded. It is also advantageous to study the crystal at higher temperatures. This can yield information about the levels near the ground state. In an attempt to compile a maximum amount of data on the crystal, experiments were made at liquid helium, liquid nitrogen and room temperatures. However, signals recorded at higher temperatures were not used in the final analysis because they were too weak.

With these ideas in mind, we can move on to examine how the experiment was designed and run. From a practical point of view, the goal of the experiment was to maximize the sensitivity of the equipment measuring the signal while minimizing the noise. Therefore, the following paragraphs concentrate on the logistics of the experiment. Naturally the optical arrangement constitutes the foundation of the experiment. However, in order to understand the design, it is helpful to discuss several aspects of the monochromator used. In addition to the optical arrangement, we must also consider the arrangement for signal processing, which is the last aspect discussed.

At the heart of the absorbtion experiment was the .85-meter Czerny-Turner Double Monochromator-Spectrometer. This instrument was produced by Spex Industries and consequently is referred to as the Spex for the remainder of the paper. In keeping with the goal of recording the best signal, it was necessary to design the optics of the experiment in such a way as to take full advantage of the Spex.

The Spex separates the many components of the electromagnetic spectrum by diffracting the signal off of a holographic grating. Figure 6 shows a top view schematic of the instrument.[15] In order to receive the strongest possible signal at the photomultiplier tube, it was necessary to fill the diffraction grating with light. This situation also had the additional benefit of improving the resolution of the signal. Recall that the resolving power of a grating is given by

$$R = \lambda / \Delta\lambda = mN \qquad 20$$

where R is the resolving power, λ is the wavelength of the diffracted light, m is the order and N is the total number of slits exposed. By inspection of equation 20 it is clear that the resolution improves upon using as much of the grating as possible. Of course if there is light beyond the edges of the grating, it can show up as unwanted noise. Fortunately the optimum situation was realized by simply

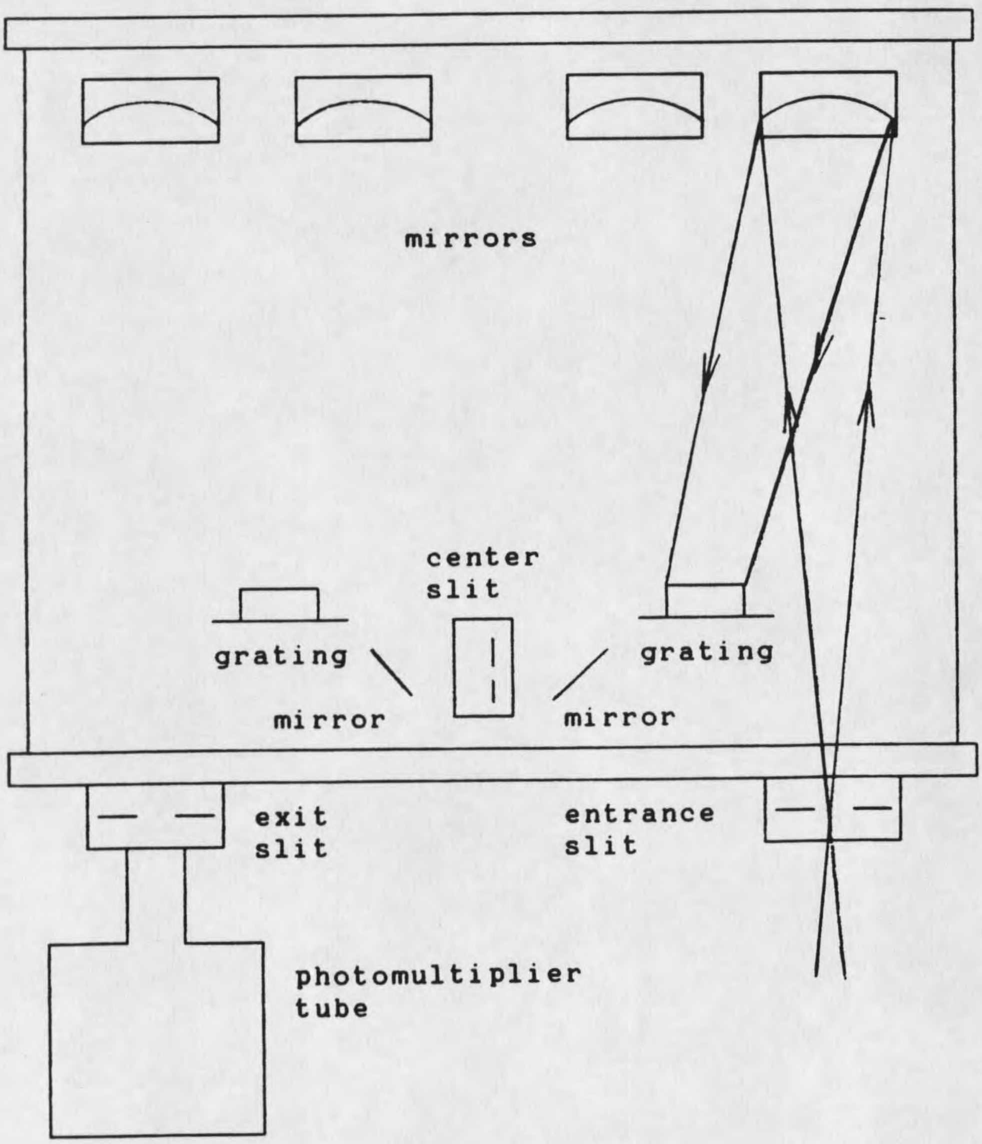

Figure 6. Top view of the Spex 14018 spectrometer used in experiments.

making sure that the signal completely filled the first mirror. This is illustrated by the rays drawn in Figure 6.

Designing the optics to send the signal from the crystal to the spectrometer begins with the first mirror in the Spex. This was easily accomplished due to the fact that the speed of the mirror was given as f/7.8. Recalling that the speed of a mirror relates the focal length and aperture size, it can be seen that the relation for finding the angle between the peripheral rays is given by

$$\theta = 2\arctan(\tfrac{1}{2}a/f) \qquad 21$$

where f is the focal length and a is the aperature of the optic.

Figure 7 shows the actual optical arrangement. Since θ is dependent only on the speed of the mirror or lens, it is clear that the effective speed of lens 3 in Figure 7 must be f/7.8. By effective speed it is meant that the actual diameter of the signal traveling from lens 2 to lens 3 is used to find the speed, instead of the physical size of lens 3. This situation was a consequence of the combination of lenses used. The parallel rays running between lens 2 and lens 3 were achieved by positioning lens 2 with its focal point on the crystal. In addition this had the advantage of maximizing the signal. It may also be noted that the positioning of these lenses was achieved by focusing a telescope on infinity and then sighting through

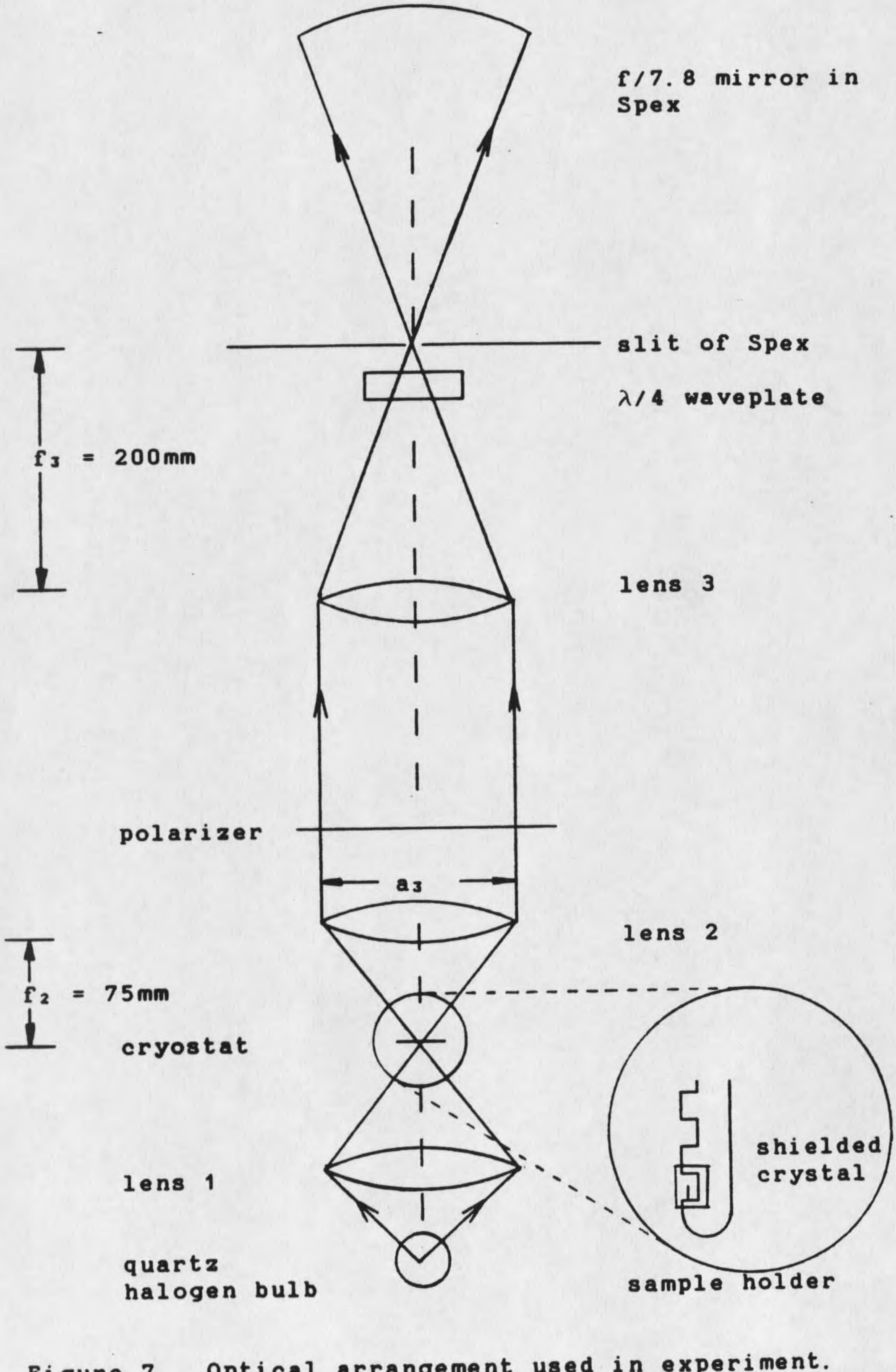

Figure 7. Optical arrangement used in experiment.

the lenses focusing on the crystal and then the Spex slits.

The next phase of the optical arrangement includes the crystal, cryostat and light source. The light source was a quartz halogen bulb focused onto the crystal by lens three as seen in Figure 7. In order to shield unwanted white light which does not pass through the crystal, the crystal was positioned over a slit of comparable dimensions made from a piece of shim stock. This is illustrated in the inset of Figure 7 along with the design of the brass sample holder. Finally the cryostat was necessary to submerge the crystal in liquid helium.

The design of the cryostat is shown in Figure 8. The cryostat, referred to as a dewar, was made out of glass with three windows through which the sample could be viewed. The sample space of the dewar was usually filled with liquid helium. If the liquid helium was not well isolated from the room it would quickly boil away. Even if time was not a factor, the bubbling would scatter the signal making it very hard to see. To isolate the sample space, several other spaces were designed into the dewar.[2] The first space adjacent to the sample space is a vacuum space used to insulate. The next space is usually filled with liquid nitrogen in order step up to room temperature gradually. The last space is under a common vacuum with the first vacuum insulating space. Even with this rather elaborate insulating system, the liquid helium

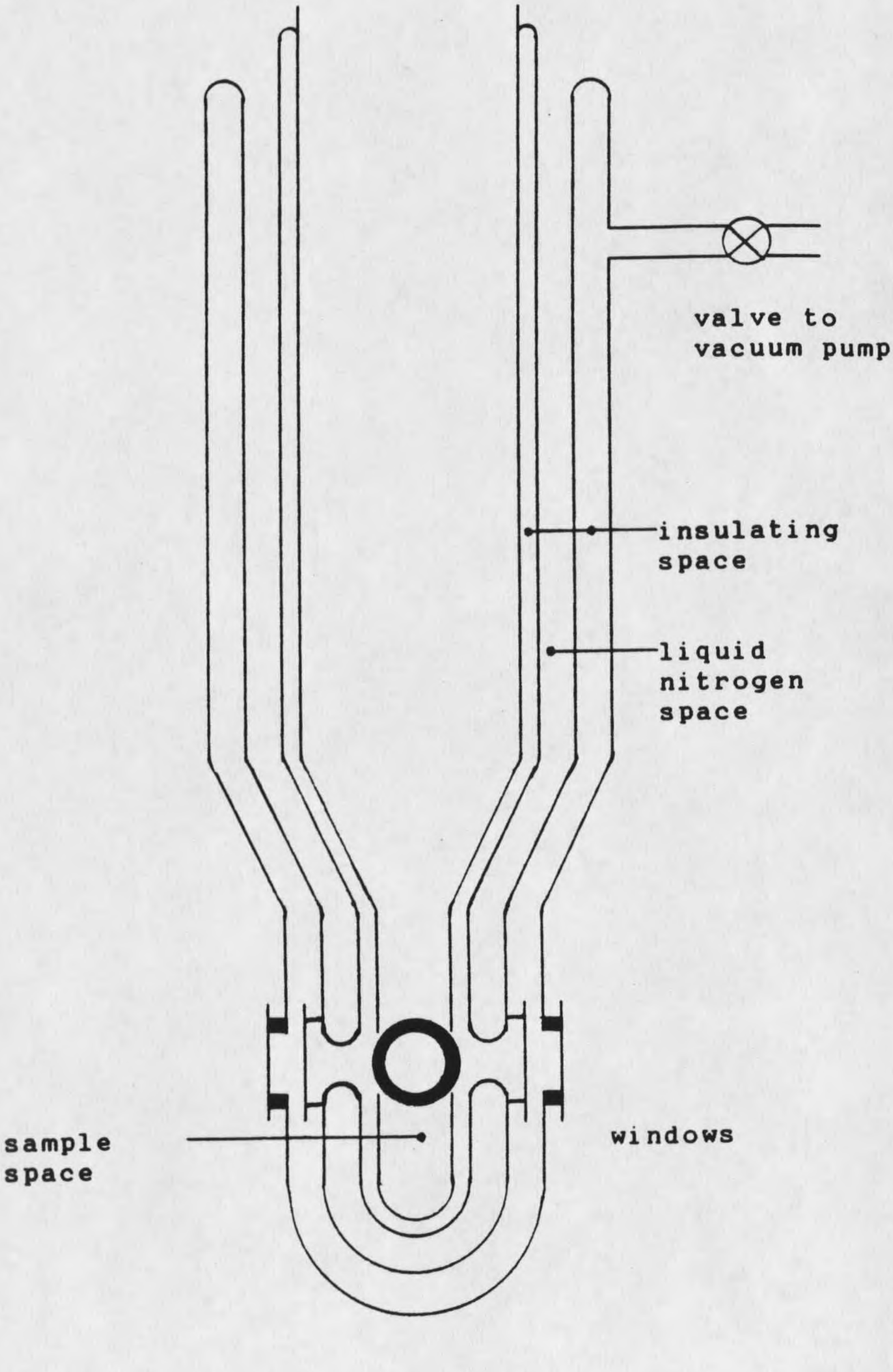

Figure 8. Cross sectional view of the glass dewar.

would still boil. To eliminate light scattering bubbles, the dewar was designed such that the sample space could be pumped. By pumping away helium vapor, evaporative cooling could take place thereby changing the helium into a superfluid. Pumping with a mechanical pump to 38 microns eliminates the bubbling.

In addition to optimizing the signal, it is also crucial to discriminate between various polarizations. Originally, the polarization was determined simply by inserting a polarizing sheet in the signal beam. Later, when reviewing contradictory data, it was found that this method of discrimination was unsatisfactory. The reason for this inadequacy stems from the poor response of the Spex in certain regions of the spectrum under different polarizations. The response of the Spex has been studied and found to respond poorly with a signal below 13000 cm^{-1} having vertical polarization.[16] The response to horizontally polarized signals was good, therefore in order to balance the response, the signal was circularly polarized. Circularly polarized light was easily achieved by inserting a quarter waveplate into the signal as shown in Figure 7.

The second part in the design of the absorbtion experiment is the signal processing which starts with the photomultiplier tube and ends with the storing of data. Figure 9 shows a block diagram for the signal processing.

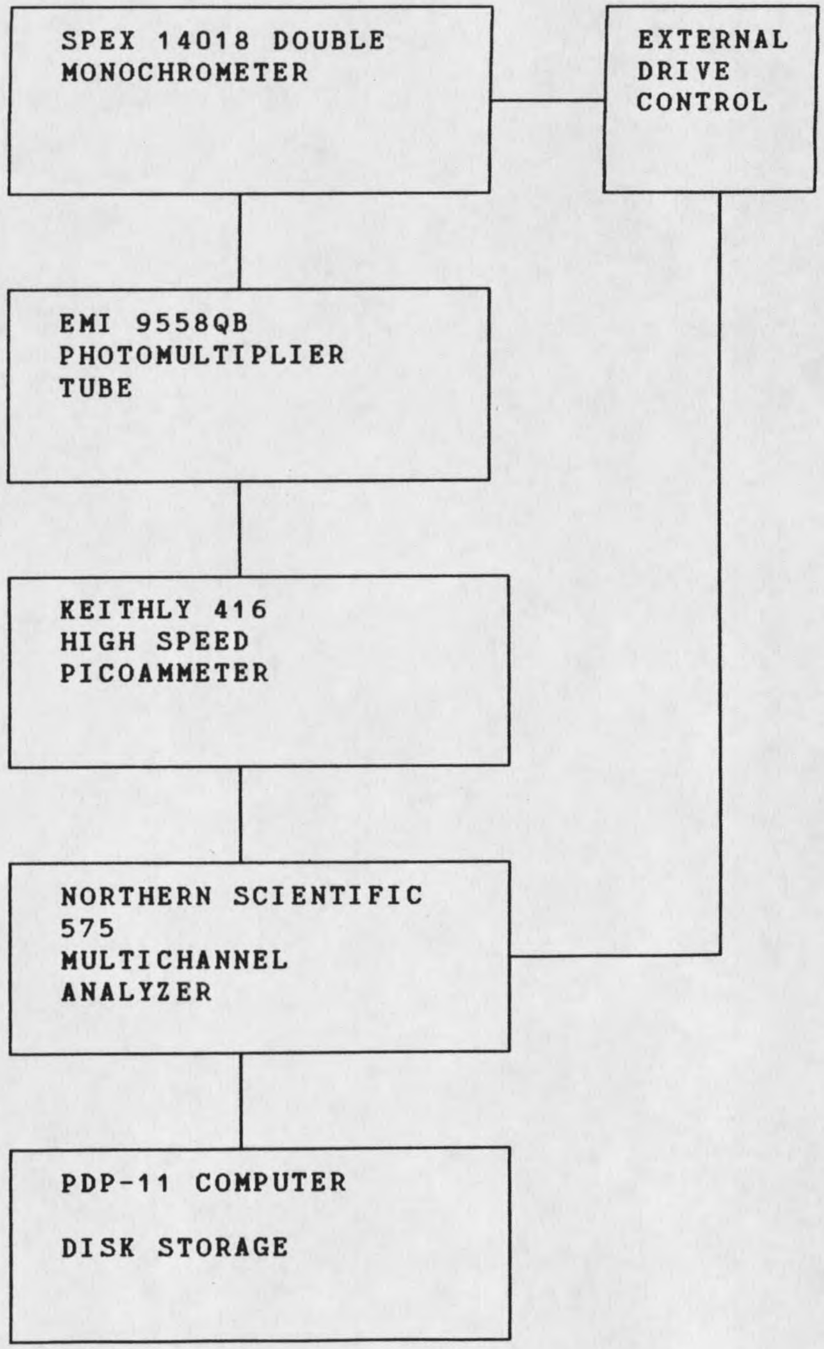

Figure 9. Block diagram of signal processing used in absorption experiment.

This diagram begins with the EMI 9558QB photomultiplier tube which initially sees the signal from the spectrometer. This signal is then sent to a Keithly 416 high speed picoammeter which in turn registers a current. By choosing the appropriate voltage applied to the photomultiplier tube, and the appropriate scale on the picoammeter, it was possible to obtain a full scale deflection on the picoammeter's panel meter. An absorption transition is found when the signal disappears momentarily while scanning the spectrum. The picoammeter then passes whatever signal it receives to the Northern Scientific 575 multichannel analyzer which is capable of storing the information digitally. The multichannel analyzer was interfaced with the stepping motor in the Spex. This allowed the instrument to scan along with the spectrometer. Because of this synchronization, it was possible to relate a particular address to the appropriate wavenumber. The last step in the process was to store the data on floppy disk. This was easily accomplished because the multichannel analyzer was interfaced to the PDP-11 computer.

The procedure used in the absorption experiment was to simply scan the spectrum for absorption lines. The first absorption line was found by trial and error. For Pr^{3+}:$Y(OH)_3$, the first line found was $^3P_0$ at 20438 cm^{-1}. After finding the first line, all subsequent experiments began by scanning $^3P_0$ to insure that the system was actually recording signals originating from the crystal. With all systems set, the tedious process of scanning and recording began. The region scanned was from 23500 cm^{-1} to 16000 cm^{-1}. Most of the absorption experiment was done at liquid helium temperatures, but some lines where recorded at 77 K. Generally however, the data at the higher temperatures was too noisy to interpret due to the nitrogen boiling.

Fluorescence Experiment

In brief, the fluorescence experiment consists of measuring and recording signals emitted by excited Pr^{3+} ions in the crystal. This means that the first step is to excite the ions. After exciting the ions, the rest of the experiment is similar in principle to the absorption experiment. In other words, from an experimental point of view, the goal is to find as many fluorescence lines as possible with the least amount of noise. In obtaining this goal, it was found that the biggest difference between the absorption and fluorescence experiments came in the signal processing techniques.

Before the fluorescence experiment could begin, it was necessary to tune the exciting laser to a wavenumber which corresponds to a fluorescence state in the ion. By examining the energy level diagram for Pr^{3+} given in the Argonne National Laboratories report[8] it was found that three states fluoresce: $^1D_2$, $^3P_0$ and $^3P_1$. To excite (or pump) the ions a tunable dye laser was set to the wavenumber of the level whose energy was determined from results of the absorption experiment. The paragraphs which follow contain a brief description of the laser used to excite the ions.

One of the most significant advances in laser spectroscopy was the advent of the tunable dye laser. It was this laser which was at the heart of the fluorescence experiment. The lasing material of the dye laser is an organic dye dissolved in ethanol. Since each dye is tunable over a finite band of frequencies, it was first necessary to choose a dye which has a range containing the desired frequency. This selection can be made by examining the tuning curves from the dye manufacture's data. The dyes used in this project were coumarin and rhodamine at 20400 cm^{-1} and 16500 cm^{-1} respectively. To understand how to tune the laser to the desired frequency, it is instructive to investigate the structure of the laser.

All of the lasers used were built at Montana State University by Dr. R.L. Cone and his previous graduate students. The design of the dye laser was based on a paper written by T.W. Hänsch in 1972.[17] The basic components of the laser are shown in Figure 10. The system begins with a repetitively pulsed nitrogen gas laser.

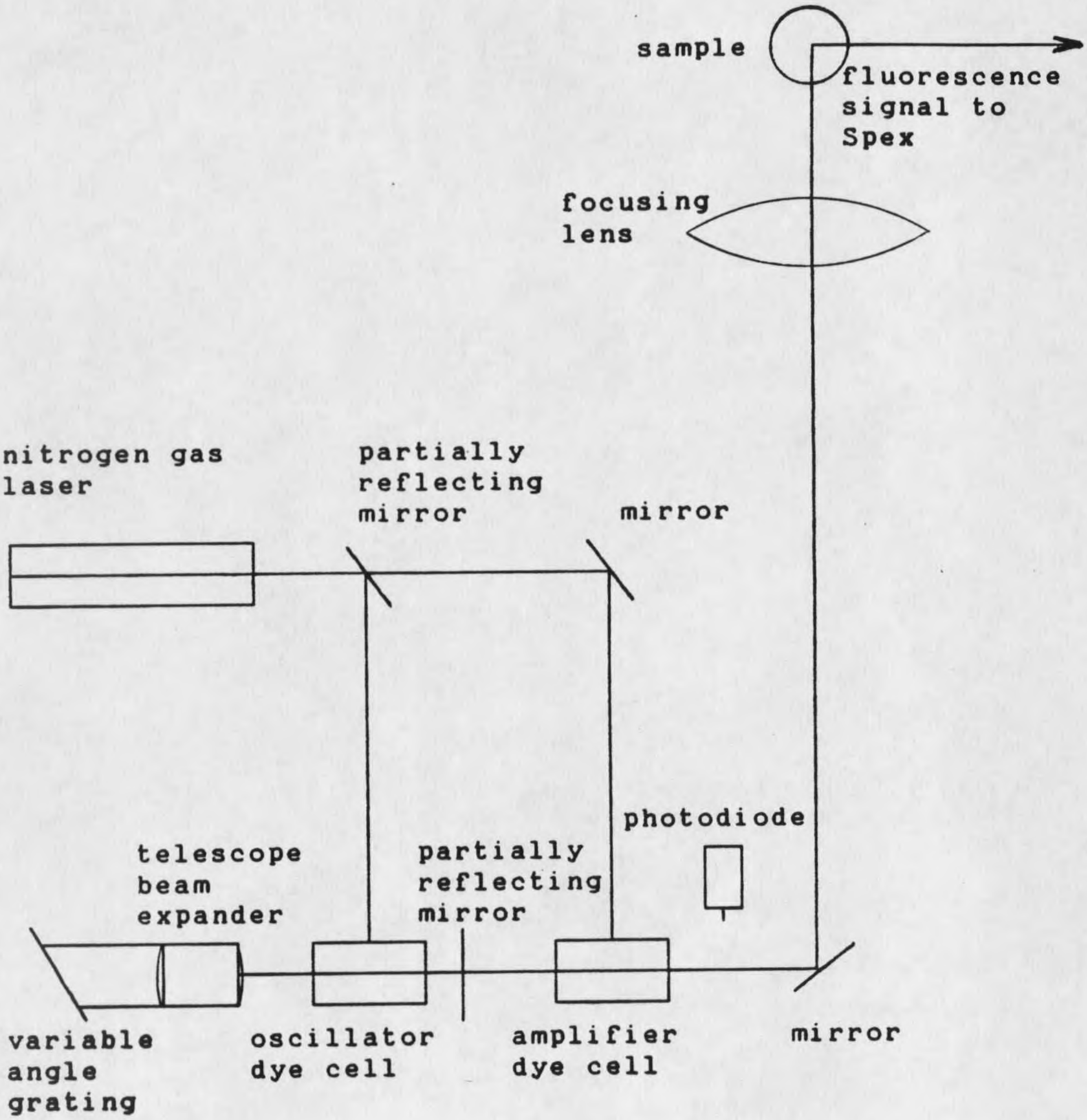

Figure 10. Schematic of system used in fluorescence experiment including the Hänsch type dye laser arrangement.

The nitrogen laser was used as the pumping source for the dye laser. The laser is basically made up of an air tight four foot long cavity with a glass window on the output end and a plane mirror on the back. The nitrogen gas is excited transversely with two pairs of electrodes running the length of the cavity. To operate the laser, the cavity is first pumped out by a mechanical vacuum pump and then nitrogen gas is allowed to flow in. To maintain a constant pressure, the chamber is slowly pumped while a fresh supply of gas continued to flow in. The pressure is typically held at 48 mmHg during operation. With a stable flow of nitrogen gas in the chamber, approximately 25 kV is pulsed across the electrodes at a repetitive rate of 6 Hz. This high voltage excites the electronic states of the nitrogen molecule. The lifetime of these excited states is quite short (on the order of 10 nsec), and consequently the nitrogen laser emits bursts of radiation typically about 10 nanoseconds long. The resultant beam is spatially fan shaped and in the violet region of the spectrum. Using mirrors on a Newport Research Corporation 4'x8' optical bench, the fan shaped beam is split up, part being directed to an oscillator dye cell and part being sent to an amplifier dye cell.

The discussion may now focus on the dye lasers. To begin with, the difference between the oscillator and amplifier cell should be clarified. Simply put, the oscillator cell is within the oscillating cavity while the amplifier is outside the cavity. The boundaries of this cavity are made up of a 632 lines per inch diffraction grating at one end and a partially reflecting mirror on the other end. Changing the angle on the diffraction grating changes the frequency at which the dye will lase. This is because the grating allows for feedback in only one particular frequency giving rise to a preferential gain at the desired frequency. As pointed out in the theory section, the best resolution from a diffraction grating can be obtained by illuminating as many lines as possible. This is accomplished by inserting a telescope arrangement between the dye cell and the grating which acted as a beam expander. The dye solution itself was contained in a cell known as a cuvette-type dye cell. This is a rectangular design which has a magnetic stirrer in the bottom to help keep the dye solution homogeneous during operation. After the beam leaves the oscillating cavity, it passes through an amplifier cell. The amplifier then simply enhances the beam. Since the experiment was dependent on tuning the laser, it is productive to outline the tuning procedure.

To set the dye laser, there must be a way to measure the wavenumber. To measure this, the beam is directed to the slit of the spectrometer which is covered by a white paper card. The card is in place to protect the spectrometer slits by diffusing the light. The signal is then seen by the Spex and consequently by the photomultiplier tube. From here the signal goes directly to an oscilloscope where it can be viewed.

To see the signal on the screen it is necessary to set the time constant on the scope. This was done by finding the RC time constant of the circuit which delivers the signal. The resistance of the circuit can be determined by simply knowing the input resistance of the scope. In the experiment a Tektronix 485 oscilloscope was used which has 50 ohm or one megohm input resistance. The value for capacitance can be determined by knowing the length of the coaxial cable used to transmit the signal. Capacitance for these cables is given as 30 picofarad per foot. The time constant generally turned out to be approximately 0.3 milliseconds using the 1 megohm input.

With the beam hitting the Spex and the oscilloscope set, the wavenumber of the laser can be found by scanning with the Spex. Once the wavenumber is found, it can be changed by adjusting a micrometer attached to the dye laser grating. Setting the wavenumber of the laser is conceptually a very simple thing to do. However in practice it seems to take at least twice as long as initially planned.

After tuning the laser, the beam was directed on to the crystal. The beam was positioned onto the crystal using a convergent lens. A logical question at this point is: how do you know when the beam is hitting the crystal? This could be determined by actually looking at the crystal and watching for fluorescence as the beam position was adjusted. This turned out to be a tedious process indeed.

The optical arrangement for the fluorescence experiment was the same as that used for absorption except that the exciting beam was incident on the crystal at 90 degrees from the optical axis in Figure 10. In principle, looking for fluorescence lines was similar to looking for absorption lines. However, the lifetime of the excited states in the ion was very short (approximately 150 nsec) and this led to a more elaborate signal processing system.

A block diagram of the signal processing system used in the fluorescence experiment is given in Figure 11. As in the absorption experiment, the signal starts at the Spex and ends as data on a disk. The first difference is found in the photomultiplier tube used. The tube used for this part of the experiment was the RCA C31034A which is a cooled tube used for weak signals. The second and major difference in the signal processing was the introduction of the signal averager. To be more precise, this instrument was known as the boxcar averager, gated integrator, produced by Princeton Applied Research Company (PARC). A gate has the effect of allowing the instruments to take data while the signal is present (gate open) and not take data in between signals (gate closed). This leads to a

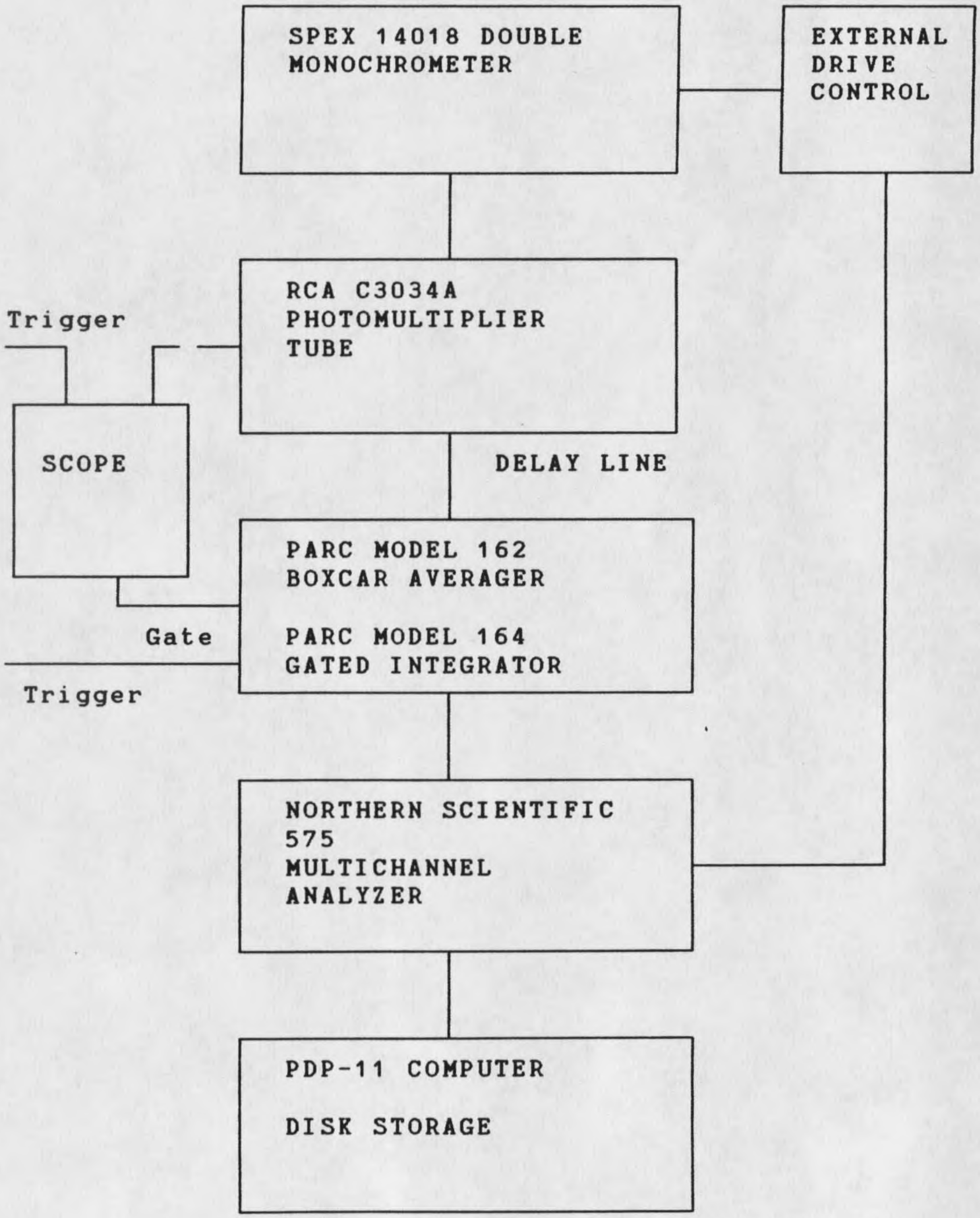

Figure 11. Block diagram for the signal processing used in fluorescence experiment.

significant reduction of noise. The boxcar was introduced because it provided a gate and could be used for very short signals. The boxcar had the additional advantage of integrating and averaging the pulse over several repetitions. To understand how the boxcar was adjusted and used, it is helpful to trace the path of the signal.

The signal began with the laser exciting the ions in the crystal. The rise time of the signal corresponds to the amount of time the laser was on which was about 5 to 10 nanoseconds. After the ions have been excited they spontaneously emit photons over a finite amount of time. This time was observed on the oscilloscope to be about 150 nanoseconds. This time should be compared to the amount of time between signals which is about 0.17 billion nanoseconds. During the time that photons are being emitted, the photomultiplier sends a signal to the oscilloscope. The signal is sent to the scope first, only to adjust the size and delay of the gate on the boxcar. So, one channel of the scope shows the signal and the other channel shows the gate. Both the scope and the boxcar were triggered by a photodiode which picked up stray light from the dye laser (see Figure 10).

At this point it is necessary to consider the amount of time it takes for the photodiode to trigger the boxcar, and consequently for the boxcar to respond. The nominal response time for the PARC 162 is 75 nanoseconds.[18]

Because of this delay in the response of the gate, the signal was arriving before the gate could be initiated. To rectify this situation, a 50 ohm delay cable was cut to a specific length in order to induce a 100 nanosecond delay in the signal. This allowed both the signal and the gate to appear on the screen of the scope. Finally the aperture duration and delay time where set to match the signal. After this adjustment has been made, the signal line was removed from the scope and put on the PARC 164 gated integrator.

The PARC 164 gated integrator operates by sampling the input signal a number of times and then computing an exponential average. Physically, this can be done by storing the voltage from each input signal on a capacitor. Unfortunately a capacitor can leak off some of its charge, particularly when the time between gates is long compared to the aperture duration. This was the case in the experiment. To solve the leaky capacitor problem, a digital storage option is available on the boxcar. This option allows one to take the analog input signal and convert it to digital format where it can be stored without loss. After averaging, the signal is converted back to analog form and sent to the multichannel analyzer.

Before leaving the boxcar averager, it is important to understand the time it takes the instrument to respond to a signal, for this directly effects the rate at which the

Spex can scan. The time it takes for the boxcar to respond is known as the observed time constant (OTC) and is calculated by[18]

$$OTC = \frac{TC}{(AD)\ (REP)} \qquad 22$$

Here AD refers to the aperture duration time, TC is the time constant selected on the instrument (1 μsec for this experiment) and REP is the repetition rate of the laser (6 Hz). For the fluorescence experiment, the OTC was typically 1.6 seconds. So, since the wavenumber spread of a signal was approximately 2 cm^{-1}, then the maximum safe scan speed for the Spex was 0.5 cm^{-1} per second. This scan speed allows the output signal to reach a signifcant fraction of its maximum gain.

After the signal leaves the boxcar, signal processing is essentially the same as in the absorption experiment. Plots for both absorption and fluorescence spectra are given in the Appendix. The primary difference between the two types of plots is the baseline. In the fluorescence experiment the baseline corresponded to zero signal and was positioned at the top of the MCA screen to reveal the negative signals. The signals were negative simple because the voltage applied to the photomultiplier was negative. The baseline for the absorption experiment appears to also be at the top of the MCA screen. In reality, the baseline was set at the bottom of the screen while the signal was blocked. This allows us to develop an idea of the strength of the absorption line. For instance, if a line hit the zero line, we could conclude that there was 100% absorption in that region of the spectrum.

To this point, the precision of the measurements has not been discussed. Because the raw data is read off the Spex, the question boils down to asking how precise the Spex is. To answer this a calibration experiment was preformed. This experiment consisted of recording the spectrum of a hollow cathode iron-neon lamp and comparing the results with those published by the American Institute of Physics.[19] After an analysis of the calibration data was done,[20] it was concluded that the wavenumber read off of the Spex was shifted by -1.83 ± 0.09 cm^{-1} from the true values throughout the spectrum.

CHAPTER 4

DATA ANALYSIS

Upon leaving the laboratory, one typically has a large quantity of data and little organization associated with it. Therefore it was necessary to first sort through the data and neatly organize it. The most efficient method found for organizing the data was to plot the spectra out and then arrange the plots in a notebook in order of their spectral range. Once it was clear what spectral lines had been recorded, a table was constructed of all possible transitions which could have produced the observed lines. Then by making guesses from the tables, a chart of experimentally determined energy levels was produced.

During the experiments, data from scanning the spectrum was recorded by the multichannel analyzer. This instrument converts an analog signal to a digital signal, and then stores the digital count in an address. The maximum number of addresses available is 1024. Therefore if we scanned over 1024 wavenumbers, then each address would store the total signal recorded after scanning one wavenumber. The raw data appears as a data address, and the actual digital count in that address. To determine the actual wavenumber where a spectral line has been recorded, it was necessary to know the initial wavenumber of the scan as well as the number of wavenumbers in each address. The algebraic expression was simply given by

$$W_s = W_i - c(A). \tag{23}$$

Here W_i is the initial wavenumber, c represents wavenumber per address, A is the address of the spectral line and W_s represents the wavenumber of the line seen. With the data in hand as well as a way to calculate the wavenumber of any line seen, it was time to plot out the data.

The absorption and fluorescence spectra were plotted on the HP7470A graphics plotter which was controlled by a Basic program run on a NEC-APCIII microcomputer. This Basic program was written by D. Macpherson, a graduate student in the Physics department. In order to generate a plot, it was first necessary to convert the data from the MCA into an x-y format. This was accomplished with a program written in the C programming language. The plots can be examined in the Appendix.

With all of the data neatly plotted it was possible to make a table containing all of the experimentally observed transitions. The crux of the situation was that the energy levels involved in each transition were yet unknown. It is at this point that the hard part of data analysis began; that is, deciding on which two states where involved in each transition.

In order to know anything about the fluorescence transitions, it was necessary to know the energy levels of the upper states. This dictated the need to label the states involved in the absorption transitions first. This was because at very low temperatures, all of the transitions could be assumed to originate from the ground state, $^3H_4(2)$. Here the μ=2 quantum number was assigned as the ground state term by inspection of Sarup's work.[13] Knowing that the initial value of energy is zero, immediately implies that the energy value seen in the transition exactly corresponds to the energy of the final state.

But how is the upper state labeled? This was done by comparing the energy found in the transition to the free ion energy. The energy levels of the free ion have been worked out in Wybourne's book[7] and an estimation of the labeled levels is given in Figure 3. After deciding on the general group which an upper level in an absorption transition belongs to, the appropriate μ quantum number had to be assigned. This was accomplished by knowing the polarization of the transition and then using the selection rules presented in Table 2. In most cases the assignment of the upper state could be made without any ambiguity due to the fact that the levels in the free ion were widely spaced. A good example of this is the assignment of the $^3P_0$ state which is somewhat separated in the spectrum at

20438 cm^{-1}. Unfortunately, the assignment of states is not always as clear, particularly if the ion did not start in the ground state. Fluorescence transitions are terminally ambiguous, so it is appropriate to discuss the assignment of states specifically for this case.

Before the ion can fluoresce, it must start in an excited state. Initially the $^3P_0$ state was pumped by the dye laser since the absorption for this level was strong. A strong absorption transition allows us to populate the upper fluorescence state with more electrons and thereby obtain a stronger signal. Because the $^3P_0$ state is pumped does not mean that all of the fluorescence originates from this state. Recalling the discussion in Chapter 2 on nonradiative transitions, it is seen that transitions could easily originate from the $^1D_2$ state. This state of affairs necessitated the listing of all possible initial and final states for each transition. An example of such a list is given in Table 3. The list was constructed by first finding the difference between the upper and lower states in the free ion which would roughly correspond to the transition seen. Then by knowing the energy level of the upper state from absorption data, the selection rules could be used to find all of the possible lower states. It was at this point that educated guesses had to be made for each transition.

Table 3. Example list of possible transitions responsible for spectral lines recorded.

Line recorded (cm^{-1})	Possible transition	Level determined (cm^{-1})
16176.6 σ	$^3P_0(0)$ - $^3H_6(2)$	$^3H_6(2)$ = 4261.7[a]
	$^3P_0(0)$ - $^3H_6(2')$	$^3H_6(2')$ = 4261.7
	$^1D_2(0)$ - $^3H_4(2')$	$^3H_4(2')$ = 296.4
	$^1D_2(1)$ - $^3H_4(1)$	$^3H_4(1)$ = 627.4
	$^1D_2(1)$ - $^3H_4(3)$	$^3H_4(3)$ = 627.4
	$^1D_2(1)$ - $^3H_4(3')$	$^3H_4(3')$ = 627.4
	$^1D_2(2)$ - $^3H_4(2')$	$^3H_4(2')$ = 586.4
	$^1D_2(2)$ - $^3H_4(0)$	$^3H_4(0)$ = 586.4
12304.8 π	$^3P_0(0)$ - $^1G_4(3)$	$^1G_4(3)$ = 8133.5
	$^3P_0(0)$ - $^1G_4(3')$	$^1G_4(3')$ = 8133.5
	$^1D_2(1)$ - $^3H_6(2)$	$^3H_6(2)$ = 4499.2
	$^1D_2(1)$ - $^3H_6(2')$	$^3H_6(2')$ = 4499.2
	$^1D_2(2)$ - $^3H_6(1)$	$^3H_6(1)$ = 4458.2
	$^1D_2(2)$ - $^3H_6(1')$	$^3H_6(1')$ = 4458.2
	$^1D_2(0)$ - $^3H_6(3)$	$^3H_6(3)$ = 4168.2[a]
	$^1D_2(0)$ - $^3H_6(3')$	$^3H_6(3')$ = 4168.2

[a] indicates the final selection.

A reasonable question at this point might be: what were the guidelines used in the selections, legitimizing the expression, educated guesses? Several guidelines are listed here in order of their importance. The first guideline is that no state with energy greater than the pumping laser's energy could be considered. A second condition considers that the spectrum was scanned only as low as 11000 cm^{-1}. Therefore, the electrons involved in the transitions had to be in the $^3P_0$ or $^1D_2$ groups initially. This suggests that there are four possible initial states given by:

$$^1D_2(0), \quad ^1D_2(1), \quad ^1D_2(2), \quad ^3P_0(0).$$

Most tables of possible transitions included all four of these initial states. However, in the end it was found that only the $\mu = 0$ states resulted in observable transitions. Finally, selections were made by again consulting Sarup's paper which listed all observed fluorescence and absorption signals. Reliance on this paper was kept to a minimum since the phonons in $LaCl_3$ are different from $Y(OH)_3$.

After the data has been taken, plots made, transitions compiled and possible states involved in the transitions listed, final selections of the states involved in each transition were made. From these selections it was easy to obtain the experimental energy levels.

CHAPTER 5

COMPUTER FITTING THE HAMILTONIAN

After taking and analyzing the data, attention was directed towards finding the magnitude of the parameters in the Hamiltonian. In short, this was done by initially guessing the magnitude for each parameter and then solving the Hamiltonian for its eigenvalues. With the calculated eigenvalues in hand, it was possible to compare these values to those obtained experimentally. Measuring the fit was done by a least squares analysis. The fit generally was unsatisfactory which meant that the parameters had to be adjusted and the calculation repeated. Recalling that the full form of the perturbing Hamiltonian has 18 parameters, it is clear that calculating the eigenvalues even once is a time consuming task. The process of finding the appropriate Hamiltonian may require that this calculation be repeated hundreds of times. Fortunately I was provided with a computer program written by a group at Argonne National Laboratories.[8] To insure that the program was functioning properly as well as gaining familiarity with the effects of varying different parameters, data from a known example was given to the computer and a fit for the Hamiltonian was found. With this done, my data was used in the program to seek the appropriate Hamiltonian for $Pr^{3+}:Y(OH)_3$.

The Fitting Program

The program was written in fortran and run on a VAX 11/780 computer. Its basic purpose was to calculate the eigenvalues and the eigenvectors of the $4f^2$ configuration. The $^1S_0$ level was not calculated since a transition from this level to the ground state would produce a spectral line above the visible region. In addition to calculating the levels, the program did a least squares fit to the experimental data. Based on the fit, the program would adjust any parameters which the operator had specified as variable, and then repeat the calculation. The operator was free to vary as many parameters in the Hamiltonian as desired. Another possibility was to vary one parameter while holding one or more other variables in a constant ratio to it. The maximum number of iterations the program would execute was specified by the operator. In this work, eight iterations was specified as the maximum. Rarely did the program actually complete the maximum number of iterations. This was because it terminated as soon as the change in the variable parameters became small enough such that the fit was unaffected.

Monitoring the performance of the program was the responsibility of the operator. There were several quantities calculated during each iteration that were helpful in monitoring the fitting process.

Probably the most important check to make was to be sure that the calculated ground state matched the one determined by Hund's rules. However, Hund's rules determine only the free ion term notation of the ground state and say nothing of the μ quantum number. The μ number was obtained by analysis of previous work on trivalent praseodymium[13] and from examining unambiguous transitions seen. The confirming transition seen was an absorption line at 20438 cm^{-1} with a σ polarization. By inspection of the free ion energy levels and the selection rules, it is seen that the only states giving rise to this transition would be $^3H_4(2)$ and $^3P_0(0)$. Since the line was recorded with the crystal at liquid helium temperatures, it is clear that the ground state has a μ quantum number of 2. Recalling the discussion in Chapter 4, it is clear that a different ground state erodes the credibility for most of the other selections made. So upon finding a shifted ground state, the run was immediately abandoned and the responsible parameter was noted. This situation occurred many times.

Each time the program changes a specified parameter, it calculated an error bar for the parameter varied. If the error bar grew to a significant fraction of the parameter itself, the fit was viewed with skepticism. This quantity usually remained under ten percent of the varied parameter and was not a significant problem during the many runs made.

Finally, the least squares fit quantity σ, was followed very closely. As long as all other indications are reasonable, the fit had the last word as to the performance of the run. In fact, the goal of the project was to feed all of the data collected from the experiments, and obtain a minimum in σ. But σ will never be zero. This is because there are always some errors in both the theory and the measurement. For example it is clear from examining the plots in the Appendix that not all of the lines look like delta functions. Broad lines can easily produce errors in the determination of a line.

Fitting to Data from $Pr^{3+}:LaCl_3$

The first step in the computer fitting procedure was to make sure the program was functioning properly and to gain familiarity with the Hamiltonian. This was done by entering data for $Pr^{3+}:LaCl_3$ from Sarup's work,[13] and using the free ion Hamiltonian parameters given in the Argonne National Laboratories (ANL) report.[8]

To begin with, 45 of the 60 possible levels (not including $^1S_0$ term) were entered into the program along with the free ion parameters from ANL. The free ion parameters were assumed to be reasonably close so attention was directed first towards the crystal field terms. Sarup's paper gives values for the field parameters, so $B^6{}_6$ and $B^6{}_0$ were entered using the given values while $B^2{}_0$ and $B^4{}_0$ were entered as arbitrary numbers. The first run consequently focused on the effects of varying $B^2{}_0$ and $B^4{}_0$. These crystal field parameters were chosen first because they have nonzero matrix elements for every term in the free ion. This turns out not to be the case with $B^6{}_6$. The results of this run showed that the program quickly converged on the values for $B^2{}_0$ and $B^4{}_0$ reported by Sarup. Numerical results can be examined in Table 4, run number 1. This Table provides an example of the type of organization used when running the program.

The second run concentrated on the effect of varying $B^6{}_0$ with $B^6{}_6$ in constant proportion to it. This idea of using constant proportions arose from discussions with Dr. R. L. Cone after reviewing the results from other crystals.(2) As in run 1, convergence came quickly and the values closely matched those given by Sarup. The results of this run are given in Table 4, run number 2. Notice that the values for $B^2{}_0$ and $B^4{}_0$ had been updated with those obtained in run number 1.

After varying the crystal field parameters, I began to vary the free ion parameters starting with the spin-orbit parameter. Starting with the values given in the ANL

Table 4: Numerical results from fitting program using data from $Pr^{3+}:LaCl_3$.

RUN NUMBER : 1					
LUMPED PARAMETERS:				VARIATIONS:	PARAMETER ERRORS:
E_{av}	= 9928.0	M^2	= 0.986	STARTING	
F^2	= 68368.0	M^4	= 0.669	B^2_0 = 200.0	B^2_0 = 16.5
F^4	= 50008.0	P^2	= 275.0	B^4_0 = -550.0	B^4_0 = 39.0
F^6	= 32473.0	P^4	= 206.3		
α	= 22900.0[b]	P^6	= 137.5		
β	= -674.0	B^2_0	=	ENDING	SIGMA:
γ	= 1520.0	B^4_0	=	B^2_0 = 108.4	
ζ	= 750.0	B^6_0	= -677.0	B^4_0 = -320.8	σ = 19.6
M^0	= 1.760	B^6_6	= 466.0		
RUN NUMBER : 2					
LUMPED PARAMETERS:				VARIATIONS:	PARAMETER ERRORS:
E_{av}	= 9928.0	M^2	= 0.986	STARTING	
F^2	= 68368.0	M^4	= 0.669	B^6_0 = -1000.0	B^6_0 = 36.3
F^4	= 50008.0	P^2	= 275.0	B^6_0 = -.69B^6_6	
F^6	= 32473.0	P^4	= 206.3		
α	= 22900.0[b]	P^6	= 137.5		
β	= -674.0	B^2_0	= 108.4	ENDING	SIGMA:
γ	= 1520.0	B^4_0	= -320.8	B^6_0 = -677.0	
ζ	= 750.0	B^6_0	=		σ = 17.7
M^0	= 1.760	B^6_6	=		
RUN NUMBER : 3					
LUMPED PARAMETERS:				VARIATIONS:	PARAMETER ERRORS:
E_{av}	= 9928.0	M^2	= 0.986	STARTING	
F^2	=	M^4	= 0.669	F^2 = 68368.0	F^2 = 13.0
F^4	=	P^2	= 275.0	F^4 = 50008.0	F^4 = 39.0
F^6	=	P^4	= 206.3	F^6 = 32473.0	F^6 = 28.0
α	= 22900.0[b]	P^6	= 137.5		
β	= -674.0	B^2_0	= 108.4	ENDING	SIGMA:
γ	= 1520.0	B^4_0	= -320.8	F^2 = 68359.0	
ζ	= 748.0	B^6_0	= -677.0	F^4 = 50009.0	σ = 8.2
M^0	= 1.760	B^6_6	= 466.0	F^6 = 32728.0	

[a] All values in units of cm^{-1}.
[b] The program uses 1000α, which is expressed as α here.

report, the program claimed convergence within three iterations, showing almost no improvement in the fit. Numerical data from this run is not shown here, but the new value obtained for ζ was used in all subsequent runs.

The next parameters which were varied were the electron-electron interaction terms. The initial values for these parameters were those given by the ANL report. As is typical for this program, convergence came quickly. Scanning through the results, it was found that the differences between calculated and experimental eigenvalues was not constant in the sense of being all positive or all negative. On the other hand, the spin-orbit parameter produced a constant negative difference. The numerical results of this run are given in Table 4, run number 3. Notice that the improvement of the fit is considerable.

With all of the major parameters in the Hamiltonian varied and adjusted, attention was directed towards the smaller correction terms. First among these was α. Starting with an arbitrarily large value, the calculated eigenvalues showed large positive shift from the experimental values. Even with this large initial shift, convergence came within three iterations. Small correction terms similar to α are given by β and γ. By starting with arbitrarily shifted values, a large negative shift in the calculated eigenvalues was observed. Once again however, the program converged within three iterations with very little improvement in the fit. The last parameter varied independently was P^2. Following the procedure suggested in the ANL report,[8] P^4 and P^6 were held in constant proportions to P^2 during this run. Assuming this parameter would contribute little towards improving the fit, the initial value was that given in the ANL report. This run did show some change in the parameter which would suggest that it should be varied when trying to fit the $Pr^{3+}:Y(OH)_3$ Hamiltonian.

As a final test, all parameters were set free at the same time except for the M's. The M's were held constant because it was felt that these parameters would contribute very little to the fit.[2] The initial parameters used were those obtained in the first 7 runs. Convergence came quickly and the fit improved little.

In review, it was observed that the crystal field parameters and the electron-electron interaction parameters (F^2, F^4, F^6) made the most significant contributions to the fit. Additionally, by reviewing the work of J. Sugar[11] it is assumed that stronger crystal fields produce bigger shifts in energy levels, particularly the upper levels such as ^3P and ^1I. Therefore when attempting to fit the experimental data to the $Pr^{3+}:Y(OH)_3$. Hamiltonian, efforts were made to utilize these findings.

Fitting to Data from $Pr^{3+}:Y(OH)_3$

Fitting the Hamiltonian to data from $Pr^{3+}:LaCl_3$ is an admittedly artificial example. This is due to the fact that the most difficult and critical decisions had already been correctly made. Those decisions were involved with constructing a table of energy levels from the observed spectra. When fitting to $Pr^{3+}:Y(OH)_3$ data, it must be kept in mind that some of the selections may not be correct. It only takes one mislabeled level to prevent the program from finding an acceptable fit. Because of this, the process used to find the Hamiltonian for $Pr^{3+}:Y(OH)_3$ is more involved.

The selection process was complicated in this work due to the fact that $^1I_6$ and $^3P_1$ appeared to have similar energy levels. Additionally, the $^1D_2$ terms did not seem to fit. Trouble with $^1D_2$ has been common in $Pr^{3+}:LaCl_3$ and attempts have been made(21) to eliminate this problem but this work did not incorporate any of these very recent refinements. These selection problems were finally solved by excluding all experimentally determined levels from $^1D_2$, $^3P_1$ and $^1I_6$. This meant that only the most restrictive data was initially entered.

There is a lower limit on the number of levels the program needs to function properly. The program needs enough data to compare eigenvalues with such that the free ion parameters (F^2, F^4, F^6, ζ) and the crystal field parameters may be roughly determined. To adjust the free ion parameters, the program needs at least four centers of gravity. Entering one level in a free ion manifold determines that manifold's center of gravity. Since the crystal field acts to split the degeneracies in these manifolds, then it is reasonable to expect that the program must have more than one level in a manifold to determine anything about the crystal field parameters. The general condition given[2] in order to have a reasonable chance of fitting is that the total number of observed levels entered, less the number of centers of gravity determined, must be greater than four. This may be written as

$$N_{ol} - N_{CofG} >> 4 \qquad (23)$$

where N_{lo} represents the number of observed levels entered and N_{CofG} is the number of centers of gravity determined. This expression gives some basis for the number of levels which must be entered. Because of the ambiguity in the selections, the program was initially run with the bare minimum of nine levels.

In the final process of obtaining a fit, nine of the best determined levels were entered, along with values for the parameters given by Sarup and ANL.[8,13] The initial nine levels are indicated in Table 8 on pages 76 and 77. One significant problem in obtaining a fit previously was that only one or two parameters were varied in each run.

This resulted in taking too much time to find convergence. It was therefore found convenient to vary several parameters in one run.

Varying several parameters at once was not without its hazards. Because not all of the operators are completely orthogonal, it is possible to have interdependence between the parameters. The parameters F^6, α and γ turned out to show strong interdependence. So while one value grew beyond physically acceptable bounds as determined in previous work,[22] the other dependent parameters could adjust to compensate making it appear as if a fit had been obtained. This was found to actually occur in γ, so following the lead of others,[8,22] γ was permanently fixed for all runs.

After much experimentation with the parameters, it was found that varying all of the crystal field parameters and the largest free ion parameters (F^2, F^4, F^6, ζ) together produced consistent and reasonable results. With a fit obtained for the initial nine levels, other levels were slowly added and new parameters obtained.

In order to obtain a reasonable fit, the program had to be run over 200 times. Obviously it would be nonproductive and tedious to reproduce the results of 200 runs. So, this Chapter concludes with a review of the results from the final runs.

During all of the runs made with the final 19 levels, no problems, such as a shifted ground state, were observed. Therefore, attention focused on minimizing σ. Table 5 list the results obtained after varying all of the free ion parameters except for whose value was held fixed at a value given by H. Crosswhite.[22] The initial parameters in this run gave a least squares fit of 26 cm^{-1}. Within three iterations this figure had improved considerably to 7 cm^{-1}. This run provides a typical example of varying several parameters, provided that the correct levels are in place.

After varying the free ion parameters, the crystal field parameters were varied again. Keeping in mind the large changes made in all of the parameters since the first run with nine levels, very little change was recorded at this point. Finally, to assure a good fit, I returned to varying one or two parameters per run. The last run made has its numerical data documented in Table 5 run number 2. Even though many runs had been made between the two shown in Table 5, very little actually changed. At this point, a moderately good Hamiltonian was considered found.

Table 5: Numerical results from fitting program using data from $Pr^{3+}:Y(OH)_3$.

RUN NUMBER : 1			
LUMPED PARAMETERS: E_{av} = 9928.0 F^2 = F^4 = F^6 = α = β = γ = 1400.0 ζ = M^0 = 2.300	 M^2 = 1.290 M^4 = 0.874 P^2 = 119.3 P^4 = 89.46 P^6 = 59.65 $B^2{}_0$ = 321.1 $B^4{}_0$ = -1057. $B^6{}_0$ = -1133. $B^6{}_6$ = 645.5	VARIATIONS: STARTING F^2 = 68318. F^4 = 47385. F^6 = 31808. α = 26241. [b] β = -729. γ = 748.0 ENDING F^2 = 68481. F^4 = 47524. F^6 = 32115. α = 26566. [b] β = -736. γ = 747.9	PARAMETER ERRORS: F^2 = 34. F^4 = 131. F^6 = 50. α = 277. [b] β = 20. = 0.9 SIGMA: σ = 7.1

RUN NUMBER : 2			
LUMPED PARAMETERS: E_{av} = 9928.0 F^2 = 68481.0 F^4 = 47524.0 F^6 = 32115.0 α = 26566.0[b] β = -736.0 γ = 1400.0 ζ = 747.9 M^0 = 1.760	 M^2 = 0.986 M^4 = 0.669 P^2 = P^4 = P^6 = $B^2{}_0$ = 321.9 $B^4{}_0$ = -1056. $B^6{}_0$ = -1137. $B^6{}_6$ = 646.4	VARIATIONS: STARTING P^2 = 119.3 P^4 = 0.75P^2 P^6 = 0.50P^2 ENDING P^2 = 145.7	PARAMETER ERRORS: P^2 = 18.4 SIGMA: σ = 5.7

[a] All values in units of cm^{-1}.
[b] The program uses 1000α, which is expressed as α here.

CHAPTER 6

RESULTS AND CONCLUSIONS

Having presented the ideas and methods relevant to this project, I conclude by reviewing the final results obtained. The first results which should be reviewed are the final experimentally determined energy levels. Second, the energy levels as determined by calculation are presented along with σ, the least squares fit parameter. Also the magnitudes of the parameters in the final hamiltonian are given. Finally, a few comments are made in review of this thesis.

Table 6 contains the results of the absorption experiments. Examination of the spectral plots in the Appendix reveals that the line which did not work well in the computer fitting procedure was not particularly strong. The Appendix contains the spectral plots from all of the lines recorded. However, the magnitudes of the fluorescence lines are not well represented by these plots. The magnitude of the lines depended not only on the population of the state and the transition probability, but also on the voltage applied to the photomultiplier tube. For example, the voltage applied to the photomultiplier

Table 6. Absorption lines recorded and levels determined

Line[a]	Polarization	Transition responsible	Level determined[a]
22249.7	σ	$^3H_4(2)$ - $^3P_2(2)$	$^3P_2(2)$ = 22249.7
22184.7	π	$^3H_4(2)$ - $^3P_2(1)$	$^3P_2(1)$ = 22184.7
22172.0	σ	$^3H_4(3)$ - $^3P_2(1)$	$^3H_4(3)$ = 14.5
22135.7	σ	$^3H_4(2)$ - $^3P_2(0)$	$^3P_2(0)$ = 22135.7
21339.2	σ	$^3H_4(2)$ - $^1I_6(1)$	$^1I_6(2)$ = 21339.2
21086.2	σ	$^3H_4(2)$ - $^1I_6(0'')$	$^1I_6(0'')$ = 21086.2
21022.6	σ	$^3H_4(2)$ - $^1I_6(0')$	$^1I_6(0')$ = 21022.6
21001.6	σ	$^3H_4(2)$ - $^3P_1(0)$	$^3P_1(0)$ = 21001.6
20990.2	π	$^3H_4(2)$ - $^3P_1(1)$	$^3P_1(1)$ = 20990.2
20436.5	σ	$^3H_4(2)$ - $^3P_0(0)$	$^3P_0(0)$ = 20436.5
16802.2	π	$^3H_4(2)$ - $^1D_2(1)$	$^1D_2(1)$ = 16802.2
16761.2	σ	$^3H_4(2)$ - $^1D_2(2)$	$^1D_2(2)$ = 16761.2
16734.2	σ	undetermined	undetermined
16471.2	σ	$^3H_4(2)$ - $^1D_2(0)$	$^1D_2(0)$ = 16471.2

[a] all numbers in units of cm^{-1}.

when recording the lines at 16472 and 16457 cm^{-1} was around 900V. In contrast, the lines recorded with wavenumbers below 16450 cm^{-1}, were recorded with the photomultiplier at 1800V.

The results from the fluorescence experiments can be reviewed in Table 7. Note that some of the transitions recorded yielded information on the same eigenstate. This means that there were fewer levels to work with in the computer fitting procedure, but the levels used were more reliably determined.

The most strikingly contradictory line recorded was at 16457.3 cm^{-1}. Examination of the plot for this line in the Appendix shows that this fluorescence was the strongest recorded. In fact, this line was often used to adjust the instruments during the experiment. Originally the transition believed responsible for this line was $^1D_2(0)$ $^3H_4(3)$, which determined $^3H_4(3)$ to have an energy corresponding to 16cm^{-1} This seemed reasonable since this level had also been determined from absorption data. However, it was later found that when pumping the $^1D_2(0)$, the fluorescence in this region of the spectrum virtually disappeared. This suggests that the line either originates from the $^3P_0$ state or from an upper level of the $^1D_2$ term. The logical next test would be to pump an upper level in $^1D_2$. Since the magnitude of the energy level determined for this line does not match any of those expected for

Table 7: Fluorescence lines recorded and levels determined

Line[a]	Polarization	Transition responsible	Level determined[a]
18797.6	π	$^3P_1(1)$ – $^3H_5(2)$	$^3H_5(2)$ = 2192.2
16824.0	σ	$^3P_1(1)$ – $^3H_6(3)$	$^3H_6(3)$ = 4166.4
16733.0	π	$^3P_1(1)$ – $^3H_6(2)$	$^3H_6(2)$ = 4259.7
16473.0	σ	$^1D_2(0)$ – $^3H_4(2)$	$^1D_2(0)$ = 16471.2
16457.3	π	undetermined	undetermined
16270.7	π	$^3P_0(0)$ – $^3H_4(3')$	$^3H_4(3')$ = 202.8
16249.0	σ	undetermined	undetermined
16176.6	σ	$^3P_0(0)$ – $^3H_6(2)$	$^3H_6(2)$ = 4261.7
12304.8	π	$^1D_2(0)$ – $^3H_6(3)$	$^3H_6(3)$ = 4168.2
12211.5	σ	$^1D_2(0)$ – $^3H_6(2')$	$^3H_6(2')$ = 4261.5
11394.0	σ	$^1D_2(0)$ – $^3F_2(2)$	$^3F_2(2)$ = 5079.0

[a] all values have units of cm^{-1}.

praseodymium, it may be that the crystal studied had a contaminant in it such as europium.

Both the absorption and fluorescence experiments were repeated several times. Therefore most of the lines presented here were recorded on more than one occasion. One important exception to this was a line at 11394 cm^{-1}. This line was recorded during an experiment using one particular crystal and was not found in two subsequent experiments using a different crystal from the same batch of crystals. All other conditions such as crystal temperature, level pumped and photomultiplier voltage were identical. The last fluorescence experiment pumped levels ${}^{1}D_2(0)$, ${}^{3}P_0(0)$ and ${}^{3}P_1(1)$ in an attempt to clarify the selections.

As mentioned previously, the program for fitting calculated energies to experimental energies had been run many times and the final results were moderately good. However, three levels were not used in this fit so σ has a somewhat artificial value. The final least squares fit parameter with 19 levels fitting was 7.7 cm^{-1}. Table 8 lists all of the final calculated energies and the experimental levels used in the fitting process. These energies were calculated from a hamiltonian with the parameters given in Table 9 with units of cm^{-1}.

Table 8. Final calculated energy levels for $Pr^{3+}:Y(OH)_3$

Term	μ	calculated energy (cm^{-1})	experimental energy (cm^{-1})	difference (cm^{-1})[b]
$^3H_4$	2	0.0	0.0[a]	0.0
	3	5.5	15.0[a]	9.5
	2'	182.7	-	-
	3'	188.3	201.0[a]	14.5
	1	277.5	-	-
	0	456.9	-	-
$^3H_5$	3	2132.6	-	-
	2	2186.3	2194.0	7.7
	3'	2226.1	-	-
	1	2264.0	-	-
	2'	2278.4	-	-
	1'	2434.7	-	-
	0	2501.0	-	-
$^3H_6$	3	4162.9	4168.2[a]	5.3
	2	4252.6	4261.5[a]	8.9
	3'	4386.9	-	-
	0	4392.0	-	-
	0'	4420.9	-	-
	1	4472.5	-	-
	2'	4504.4	-	-
	1'	4709.4	-	-
	0''	4747.3	-	-
$^3F_2$	1	4970.4	-	-
	0	5037.9	-	-
	2	5072.3	5079.0	6.7
$^3F_3$	0	6302.4	-	-
	2	6346.8	-	-
	3	6377.2	-	-
	1	6402.0	-	-
	3'	6412.7	-	-
$^3F_4$	3	6553.7	-	-
	3'	6610.9	-	-
	2	6653.8	-	-
	0	6704.2	-	-
	1	6713.4	-	-
	2'	6800.6	-	-

[a] one of first nine energy levels used in fit
[b] difference = (experimental) - (calculated)

Table 8. Final calculated energy levels for $Pr^{3+}:Y(OH)_3$ (continued)

Term	μ	calculated energy (cm^{-1})	experimental energy (cm^{-1})	difference (cm^{-1})[b]
$^1G_4$	3	9229.8	-	-
	3'	9447.9	-	-
	0	9566.8	-	-
	2	9594.3	-	-
	1	9653.2	-	-
	2'	9788.6	-	-
$^1D_2$	0	16459.2	16471.2	12.0
	2	16803.7	16804.0	0.3
	1	16758.8	16763.0	4.2
$3P_0$	0	20425.6	20436.5[a]	10.9
$^3P_1$	0	21002.6	21001.6	-1.0
	1	20983.0	20990.2	7.2
$^1I_6$	0	21018.8	21022.6	3.8
	0'	21083.9	21086.2	2.3
	1	21322.4	21339.2	16.8
	0''	21324.5	-	-
	1'	21383.0	-	-
	2	21478.0	-	-
	3	21559.7	-	-
	2'	21576.6	-	-
	3'	21633.0	-	-
$^3P_2$	0	22118.0	22135.7[a]	17.7
	1	22181.9	22184.7[a]	2.8
	2	22250.3	22249.7[a]	-0.6

[a] one of first nine energy levels used in fit
[b] difference = (experimental) - (calculated)

E_{av}	= 9928.0	M^2	= 1.290
F^2	= 68481.0	M^4	= 0.874
F^4	= 47524.0	P^2	= 145.7
F^6	= 32116.0	P^4	= 109.3
α	= 26.566	P^6	= 72.85
β	= -735.0	$B^2{}_0$	= 321.9
γ	= 1400.0	$B^4{}_0$	= -1056.
ζ	= 748.0	$B^6{}_0$	= -1137.
M^0	= 2.300	$B^6{}_6$	= 646.4

Table 9: Final parameters for the Hamiltonian of $Pr^{3+}:Y(OH)_3$

The fit obtained in this work was not perfect. However the calculated energy levels for $Pr^{3+}:Y(OH)_3$ presented here can be considered close and should be used as a guide when searching for spectral lines in this sample. In an attempt to improve the determination of the energy levels, future experiments could pump the upper states in the $^1D_2$ manifold. This should at least yield more information on the line seen at 16457 cm^{-1}. Another experiment may be to subject the crystal to a magnetic field, thereby finding additional lines due to Zeeman splitting. Finally, if it is felt that the sample has some contaminants in it, a new sample could be obtained, using it in the same experimental procedure outlined in this thesis.

REFERENCES CITED

(1) M.S. Otteson, Ph.D. Thesis, Montana State University, unpublished (1984).

(2) Private discussion with Dr. R.L. Cone.

(3) J.D. Jackson, Classical Electrodynamics, John Wiley and Sons, New York (1975).

(4) Private discussion with Dr. J.L. Carlsten.

(5) R.L. Liboff, Introductory Quantum Mechanics, Holden-Day, Oakland, California (1980).

(6) S. Hüfner, Optical Spectra of Transparent Rare Earth Compounds, Academic Press, New York (1978).

(7) B.G. Wybourne, Spectroscopic Properties of Rare Earths, Interscience Publishers, New York (1978).

(8) W.T. Carnell, H. Crosswhite, H.M. Crosswhite, "Energy Level Structure and Transition Probabilities of Trivalent Lanthanides in LaF_3" Argonne National Laboratory Report (1977).

(9) B.R. Judd, H.M. Crosswhite, H. Crosswhite, Phys. Rev. 169 130 (1968).

(10) K. Rajnak, B.G. Wybourne, Phys. Rev. 132 280 (1968).

(11) J. Sugar, Phys. Rev. Lett. 14 731 (1965).

(12) M. Weissbluth, Atoms and Molecules, Academic Press, New York (1978).

(13) R. Sarup, M.H. Crozier, J. Chem. Phys. 42 371 (1968).

(14) R.D. Chirico, E.F. Westrum, Jr., J.B. Gruber, J. Warmkessel, J. Chem. Thermodynamics 11 836 (1979).

(15) Spex 14018 .85-meter Czerny-Turner Double Monochromator-Spectrometer, (Spex Industries Inc., Metuchen, New Jersey 1974).

REFERENCES CITED-continued

(16) J.H. Eggert, M.J. Kimlinger, R.L. Cone, "Polarization Sensitive Spectral Response of an Optical Double Monochromator with Holographic Gratings", unpublished.

(17) T.W. Hansch, Appl. Opt. 11 895 (1972).

(18) Model 162 Signal Averager, (Princeton Applied Reasearch Corporation, 1975).

(19) American Institute of Physics Handbook, 2nd ed. McGraw-Hill, New York (1963).

(20) Private discussions with M. Winkley, R. Jones.

(21) Y.Y. Yeung, D.J. Newman, J. Chem. Phys. 86 6717 (1987).

(22) H.M. Crosswhite, H. Crosswhite, J. Opt. Soc. Am. B 1 246 (1984).

APPENDIX

Experimental Plots of Spectra

The plots which follow are those obtained from the experiments and were used in the data analysis. The labeling of each plot indicate which polarization, if any was used when recording the signal. The horizontal axis of each plot is indexed in terms of wavenumbers and therefore have units of inverse centimeters. The vertical axis is indexed in counts from the multichannel analyzer. These counts were heavily dependent on the settings of the signal processing instruments and do not necessarily represent the intensity of individual lines.

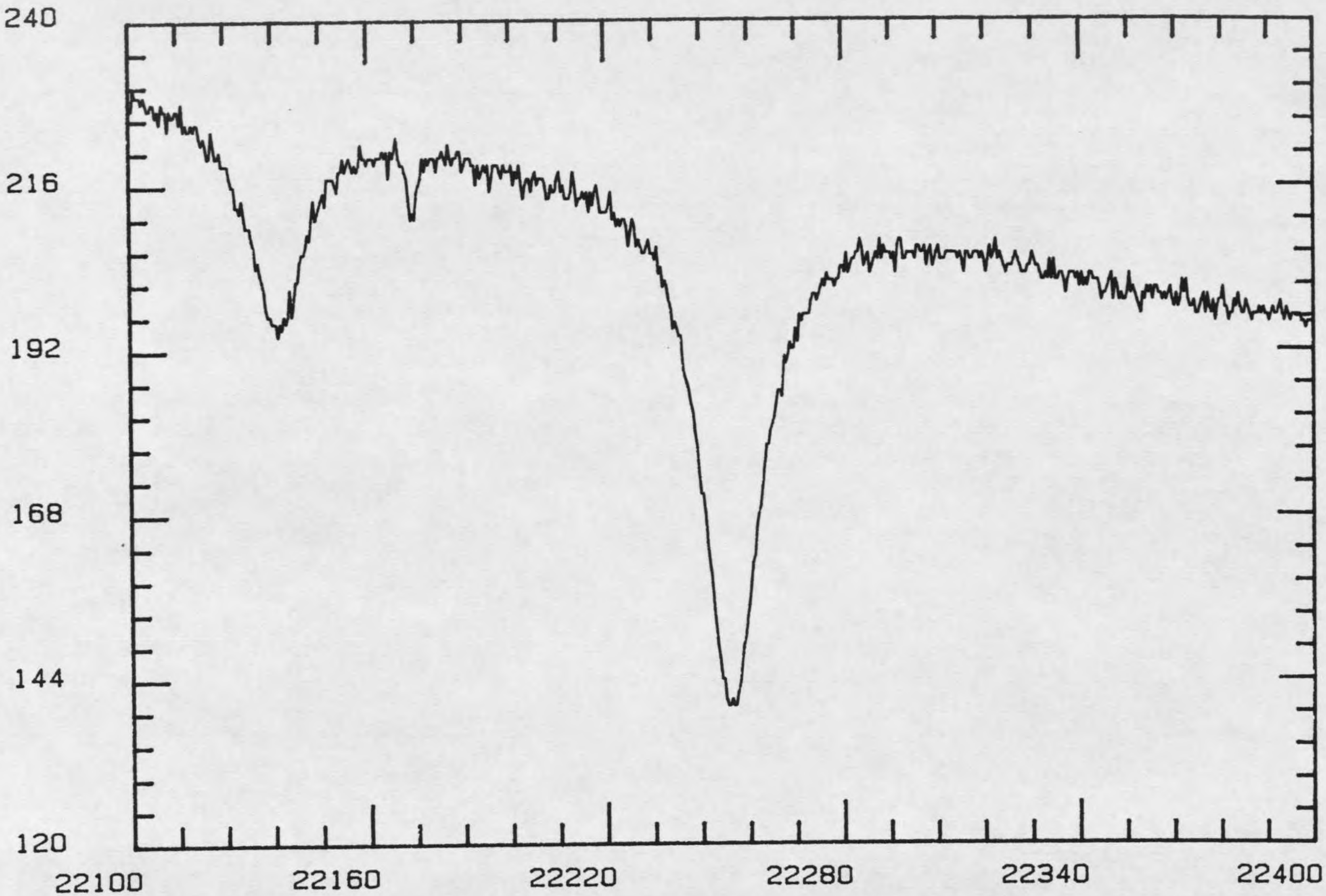

Figure 12. Absorption with sigma polarization at 22400.

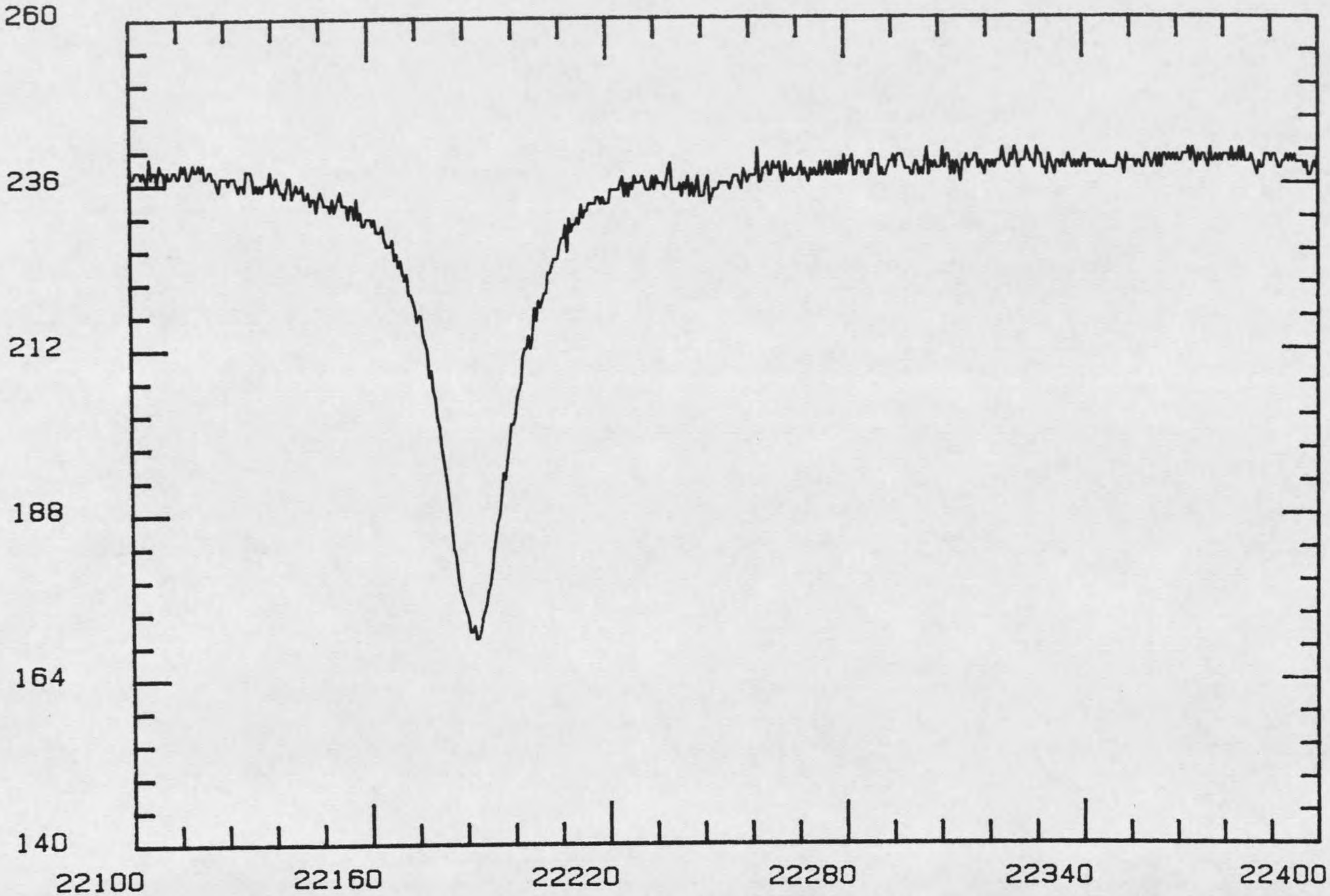

Figure 13. Absorption with pi polarization at 22400.

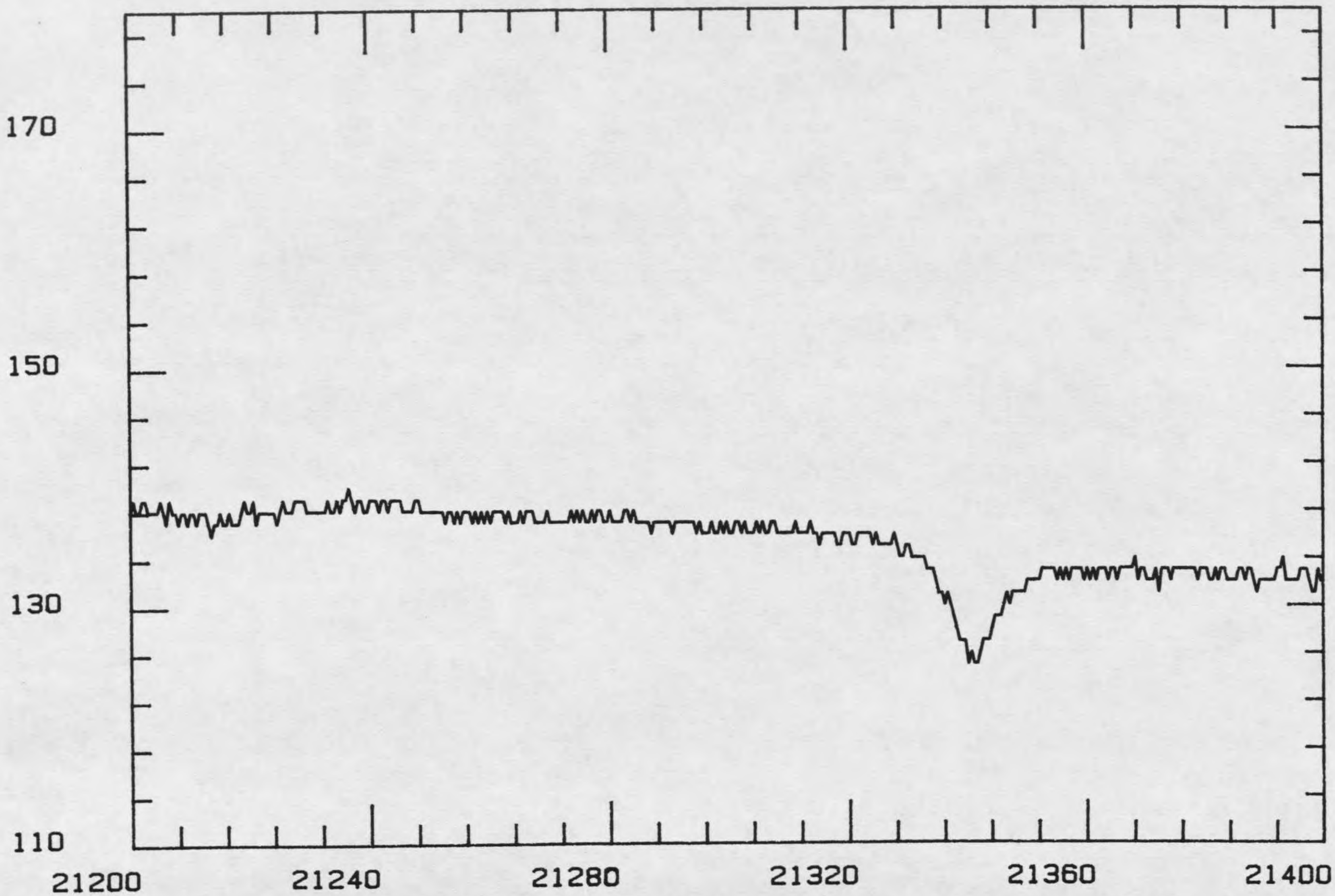

Figure 14. Absorption with pi polarization at 21400.

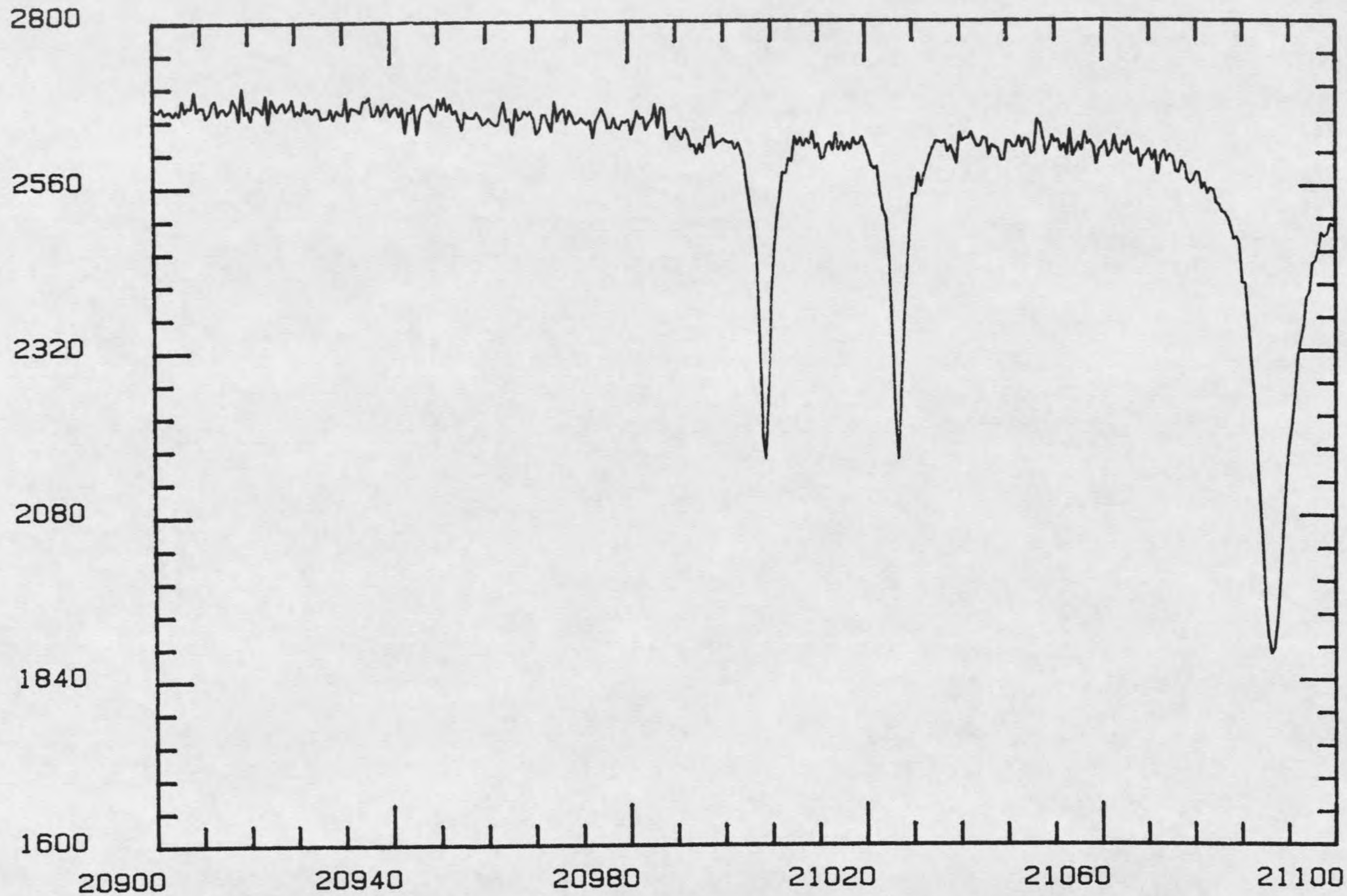

Figure 15. Absorption with sigma polarization at 21100.

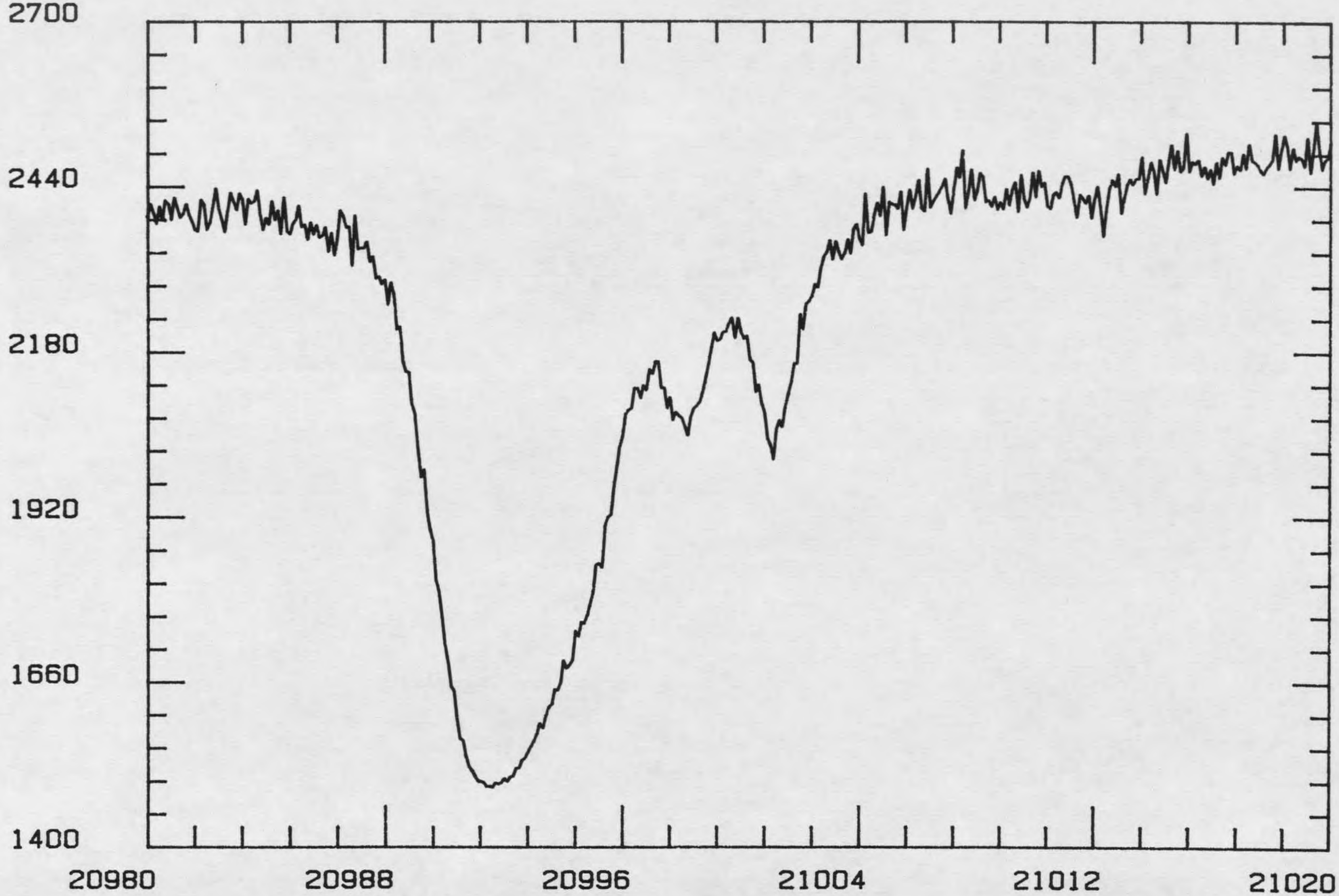

Figure 16. Absorption with pi polarization at 21020.

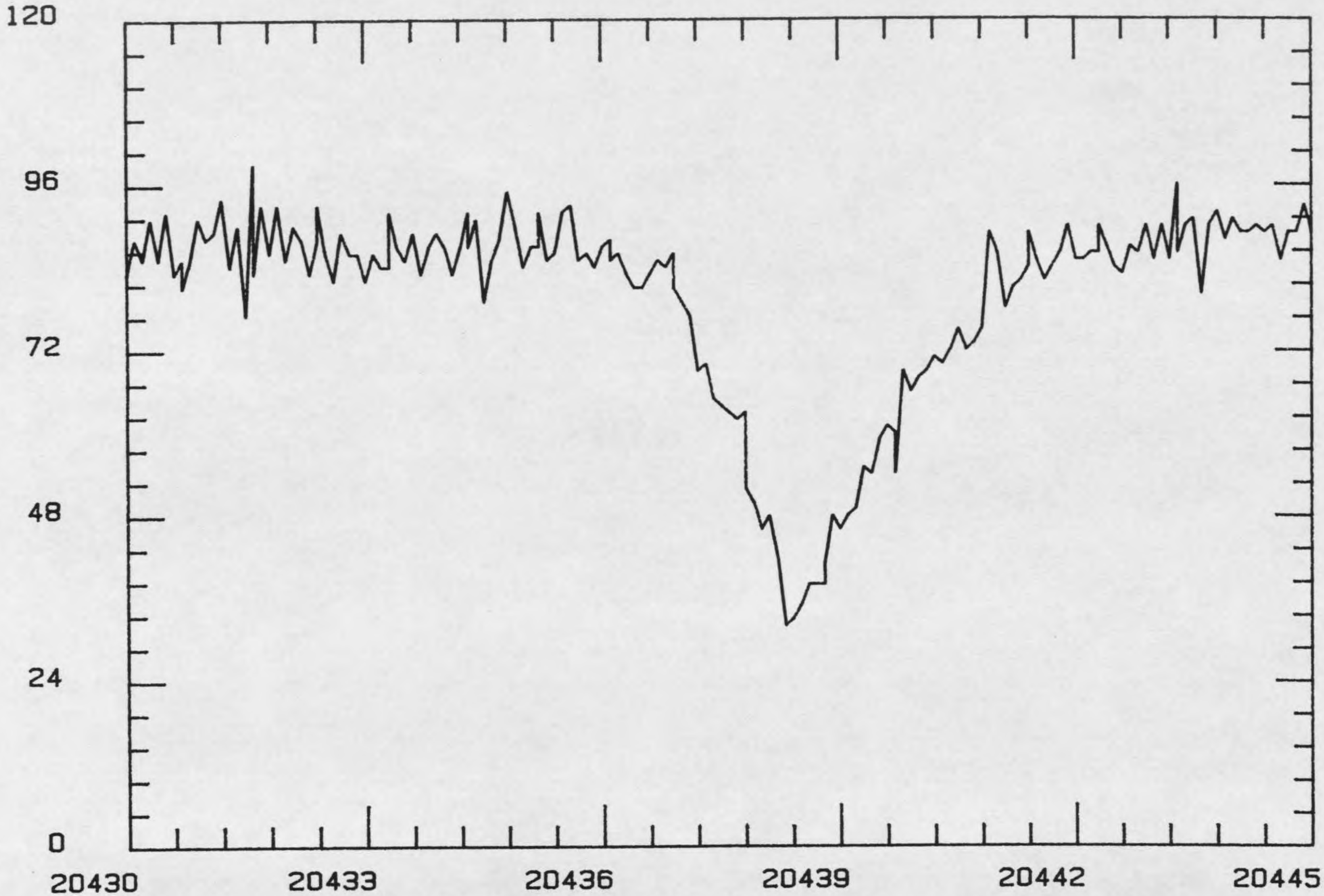

Figure 17. Absorption with sigma polarization at 20445.

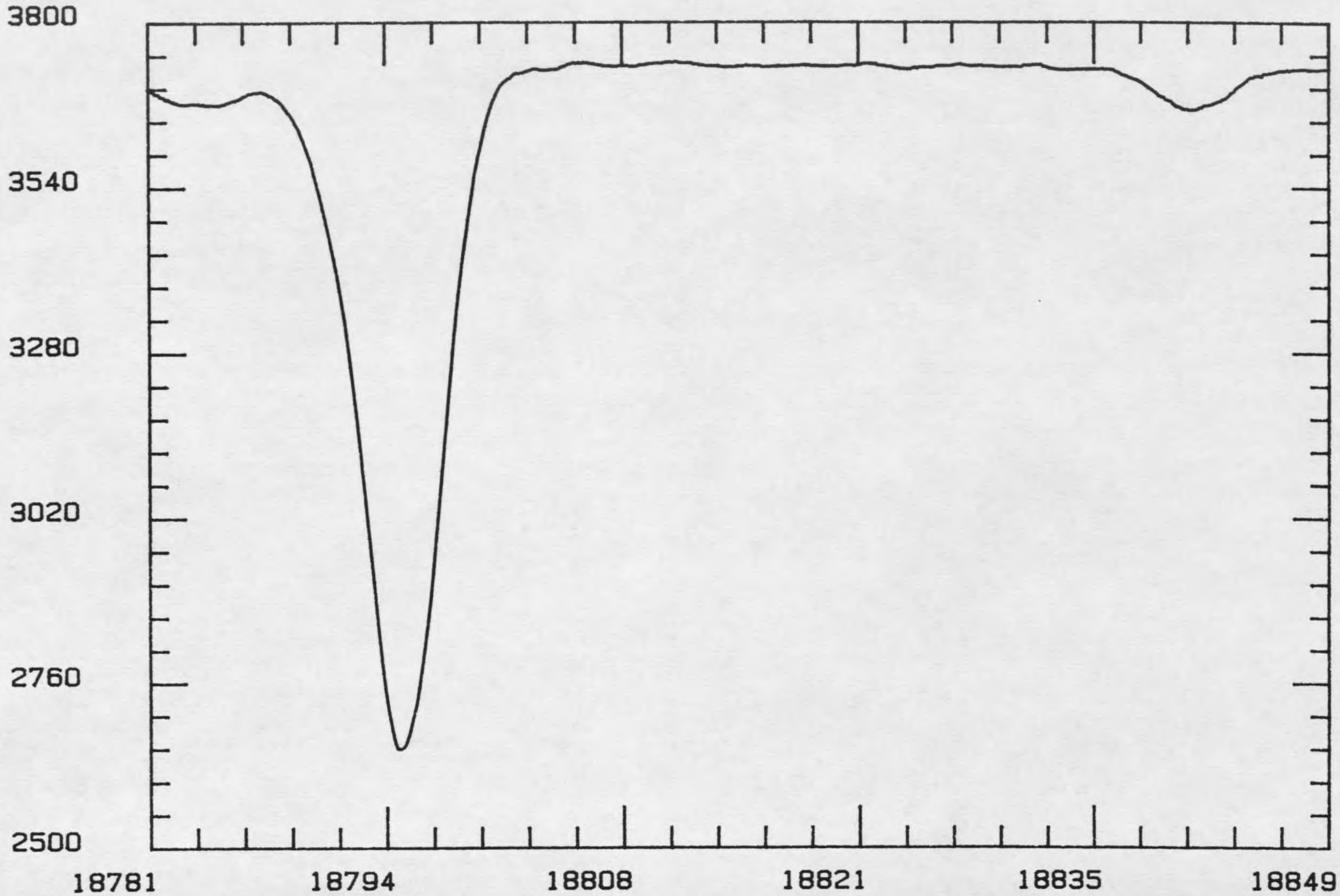

Figure 18. Fluorescence with no polarization at 18849.

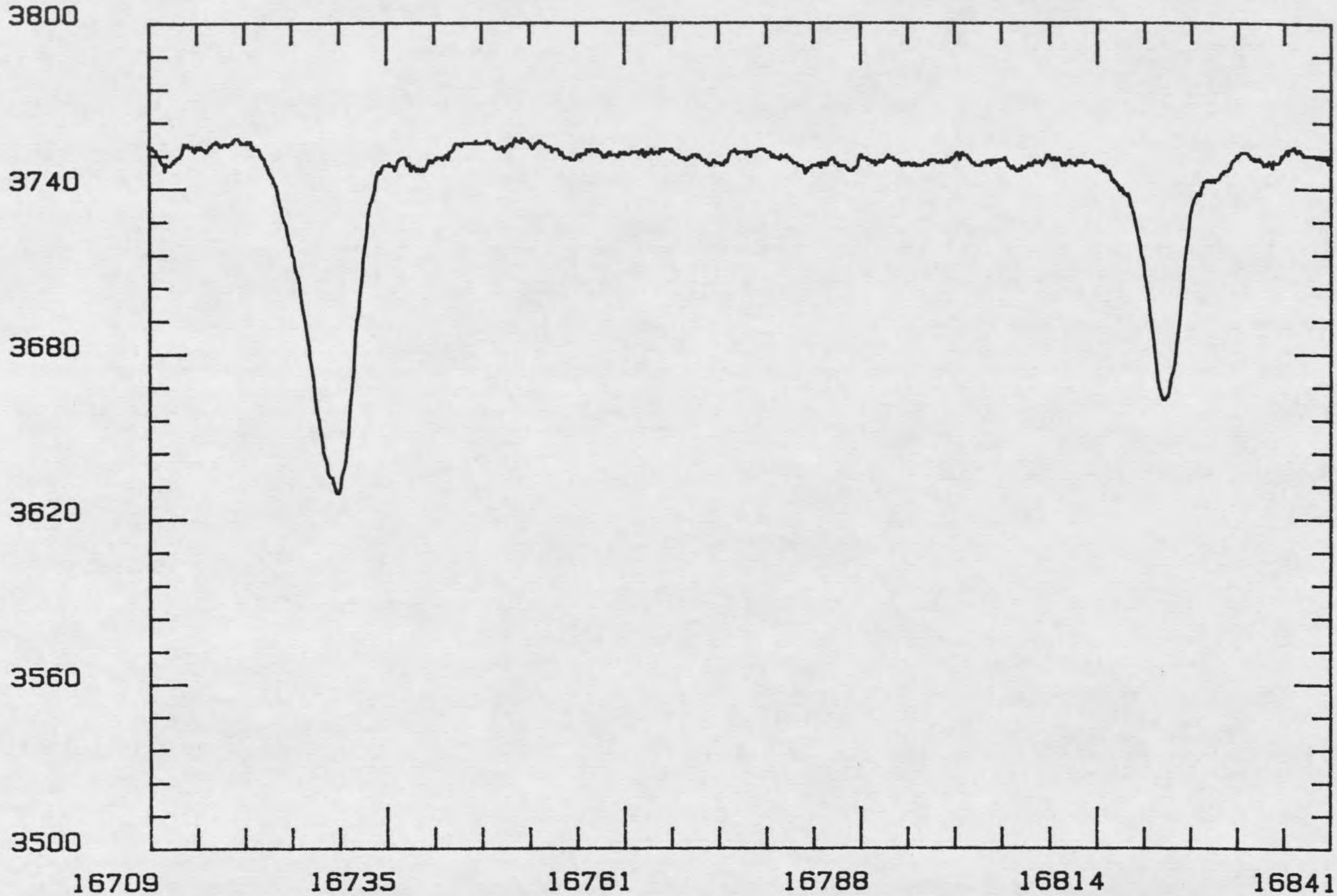

Figure 19. Fluorescence with no polarization at 16841.

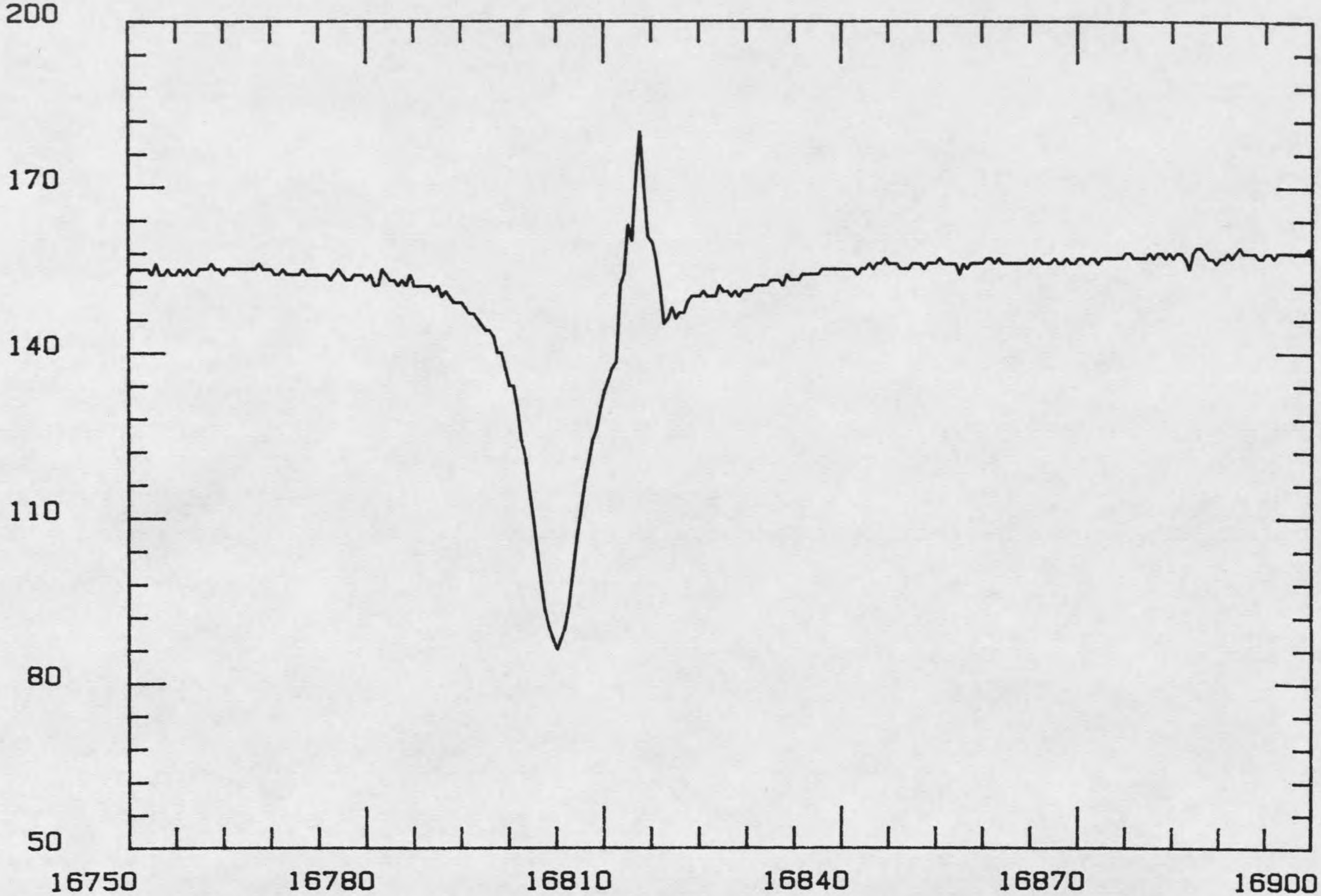

Figure 2D. Absorption with pi polarization at 16900.

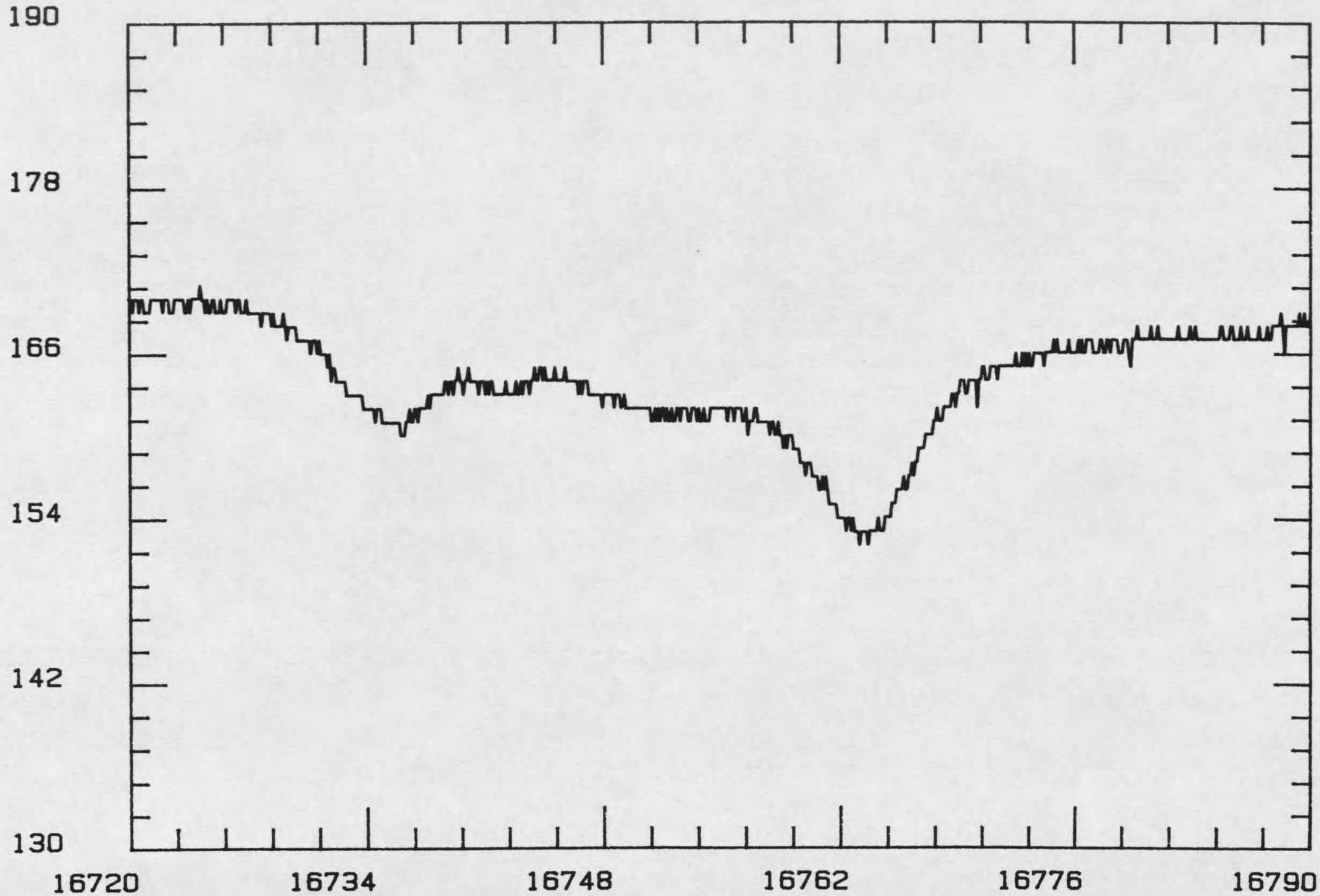

Figure 21. Absorption with sigma polarization at 16790.

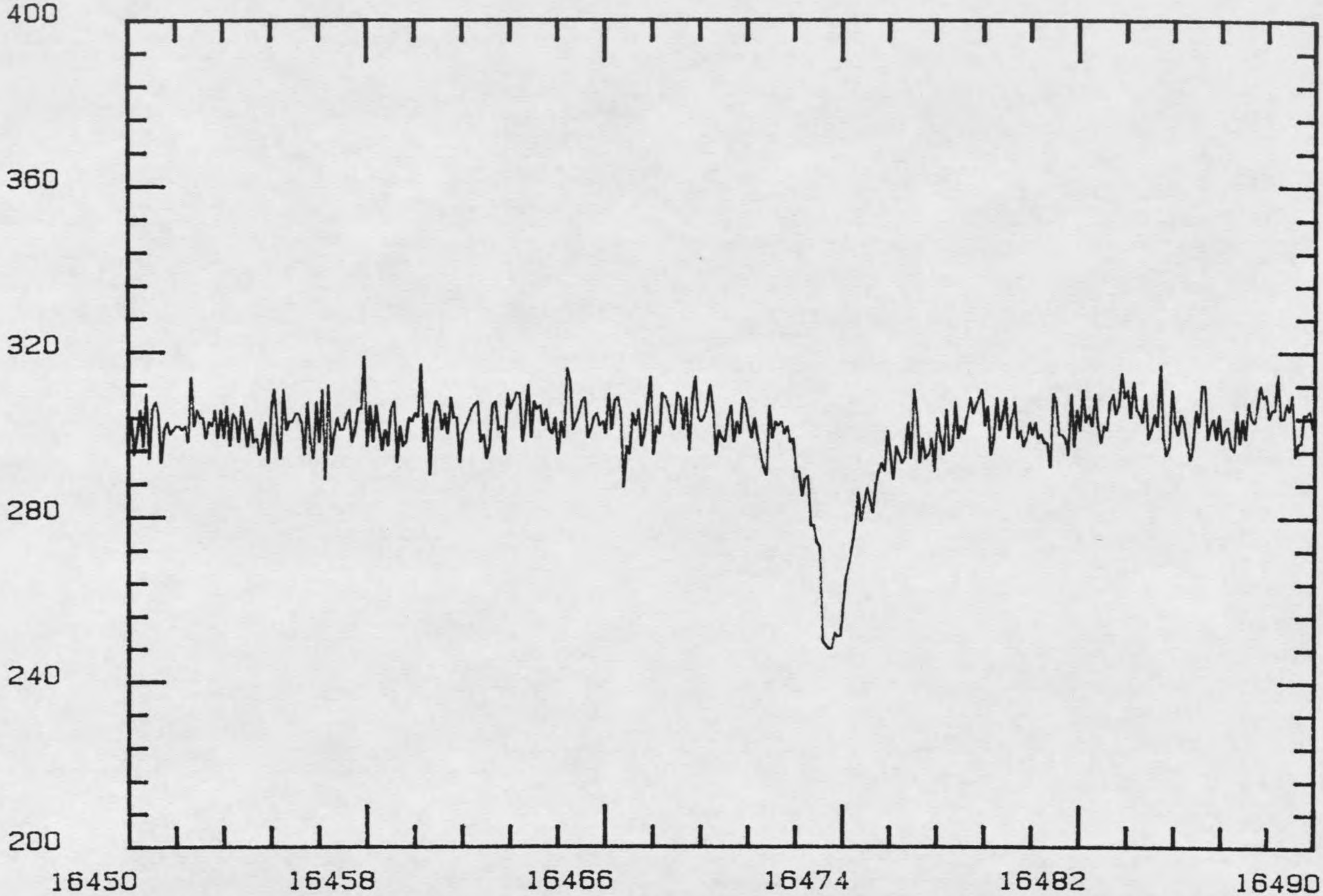

Figure 22. Absorption with sigma polarization at 16490.

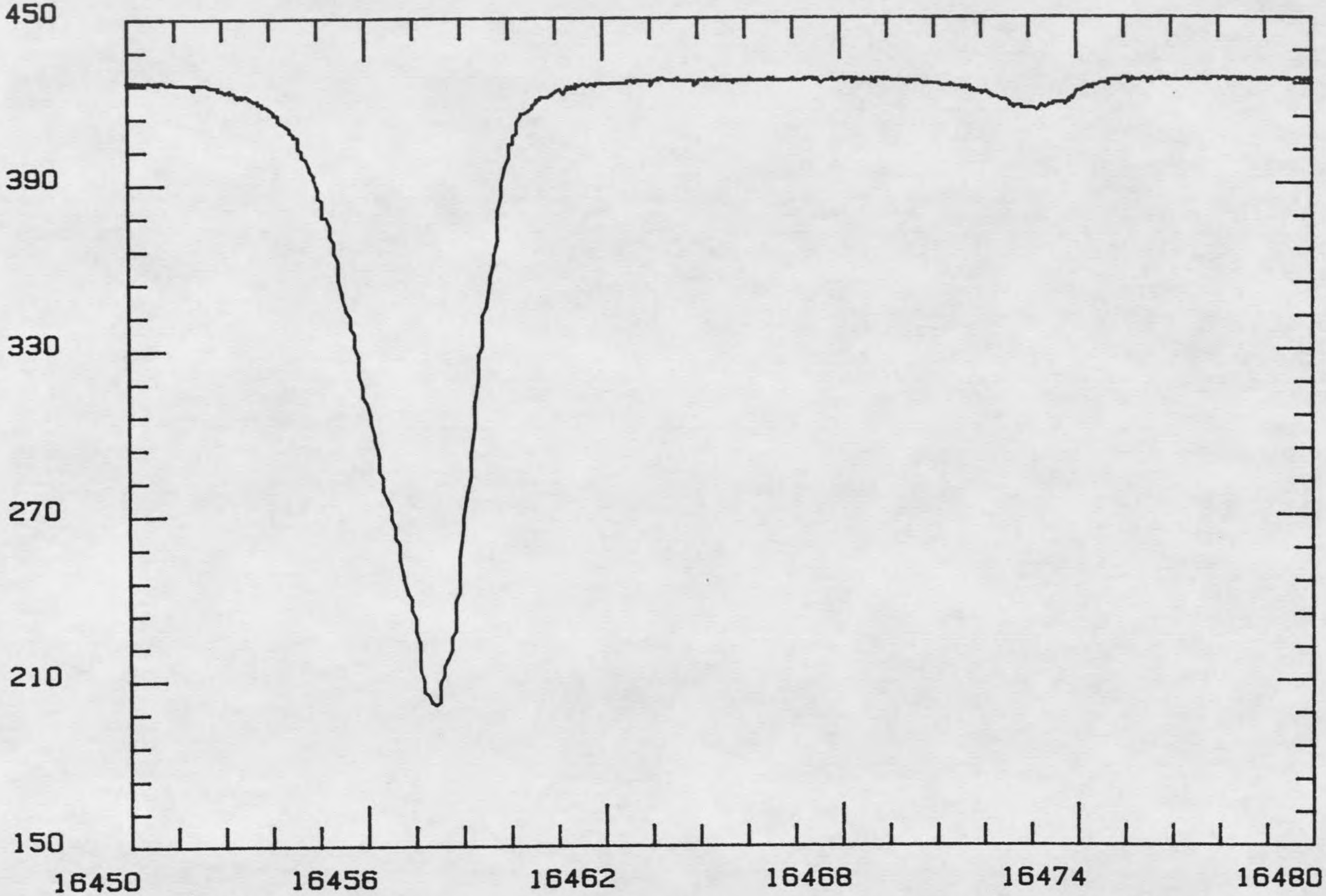

Figure 23. Fluorescence with pi polarization at 16480.

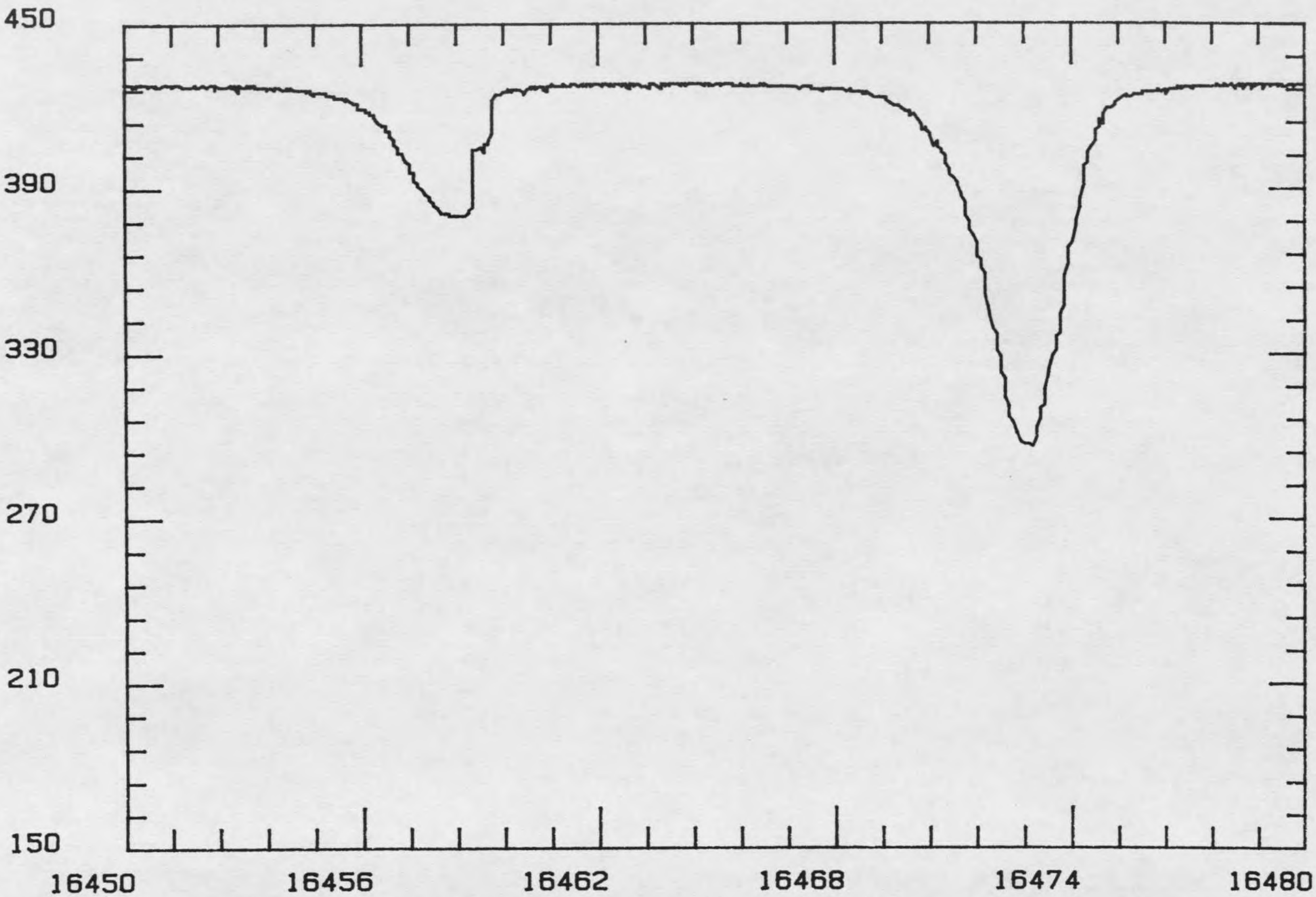

Figure 24. Fluorescence with sigma polarization at 16480.

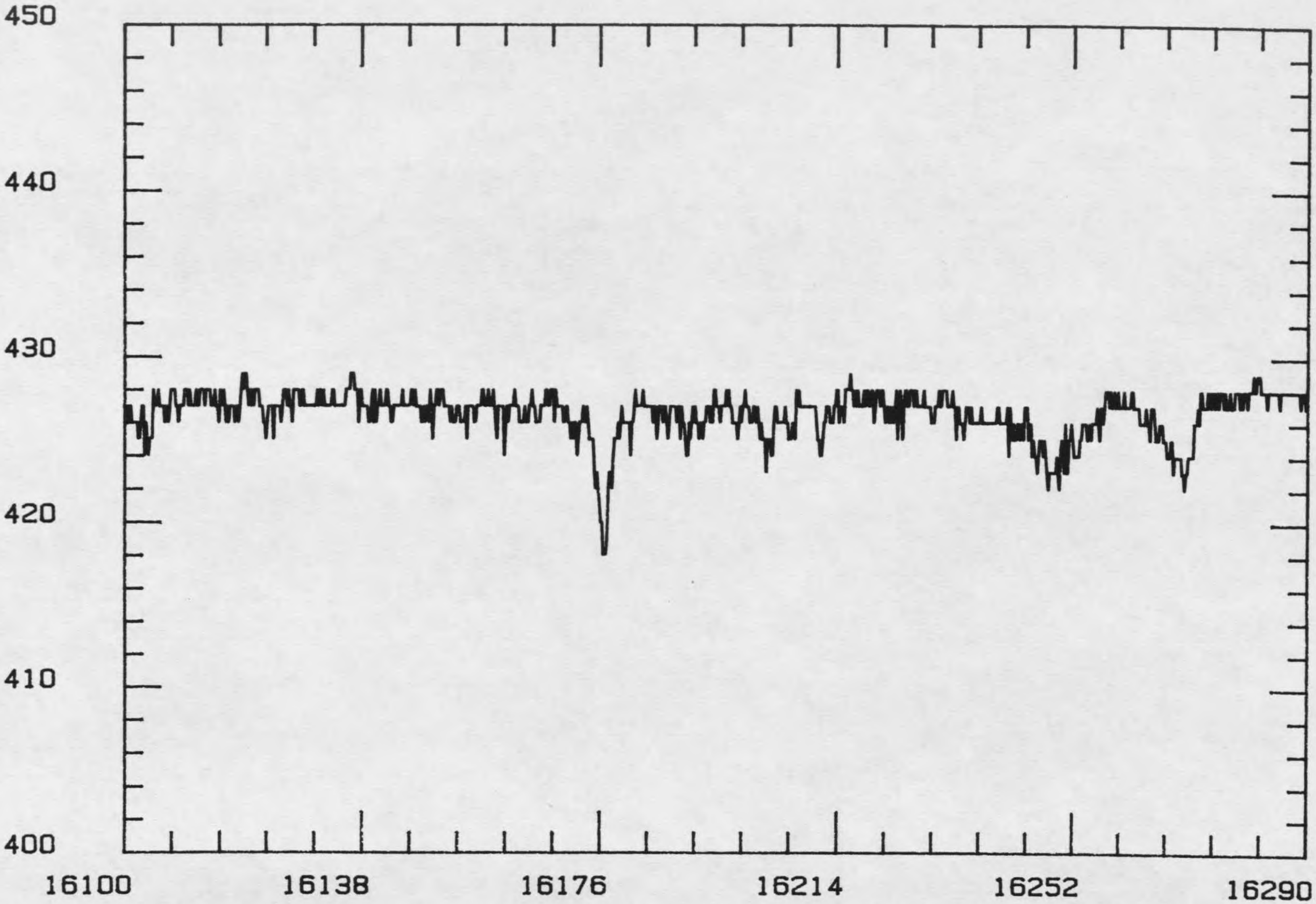

Figure 25. Fluorescence with sigma polarization at 16290.

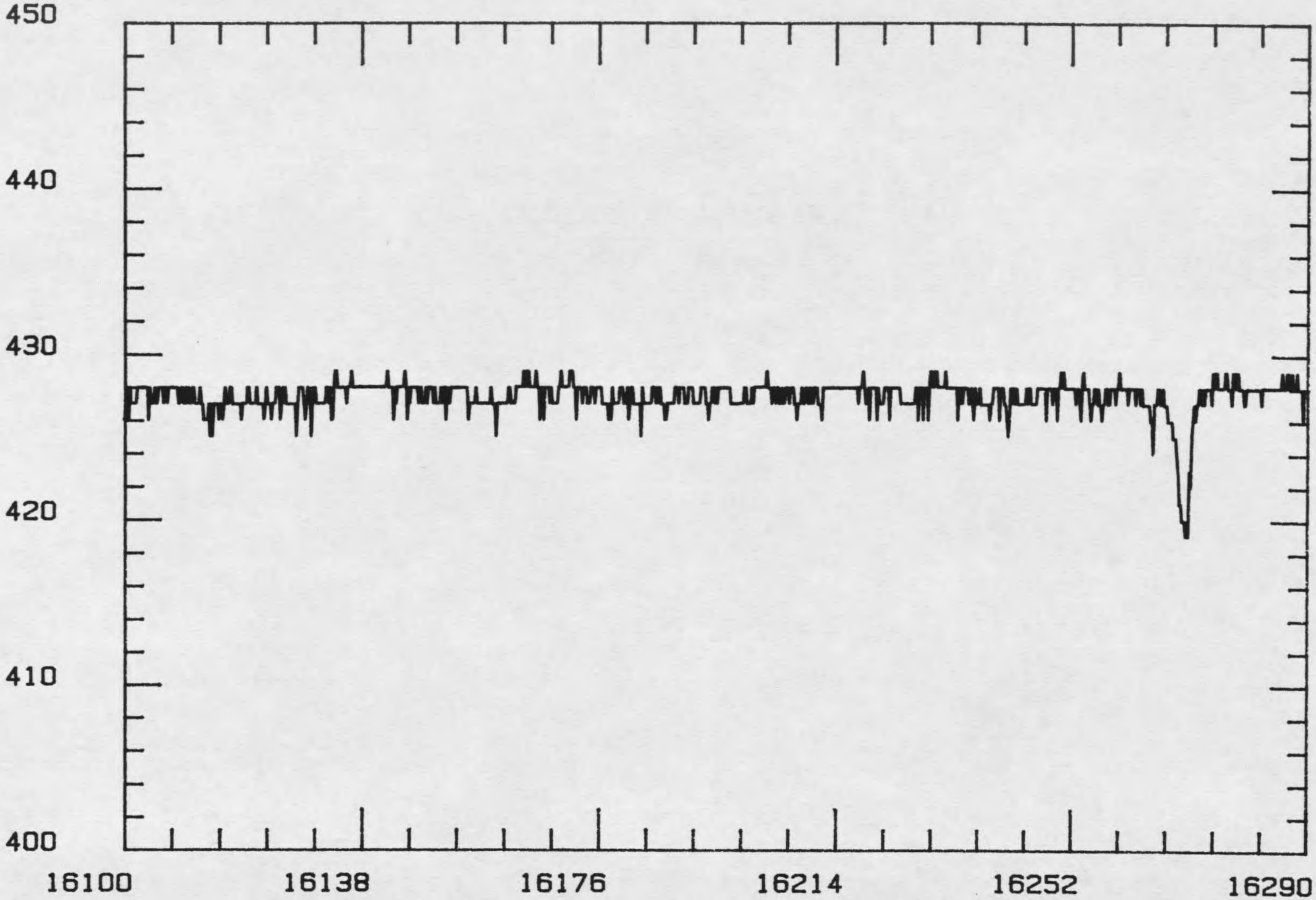

Figure 26. Fluorescence with pi polarization at 16290.

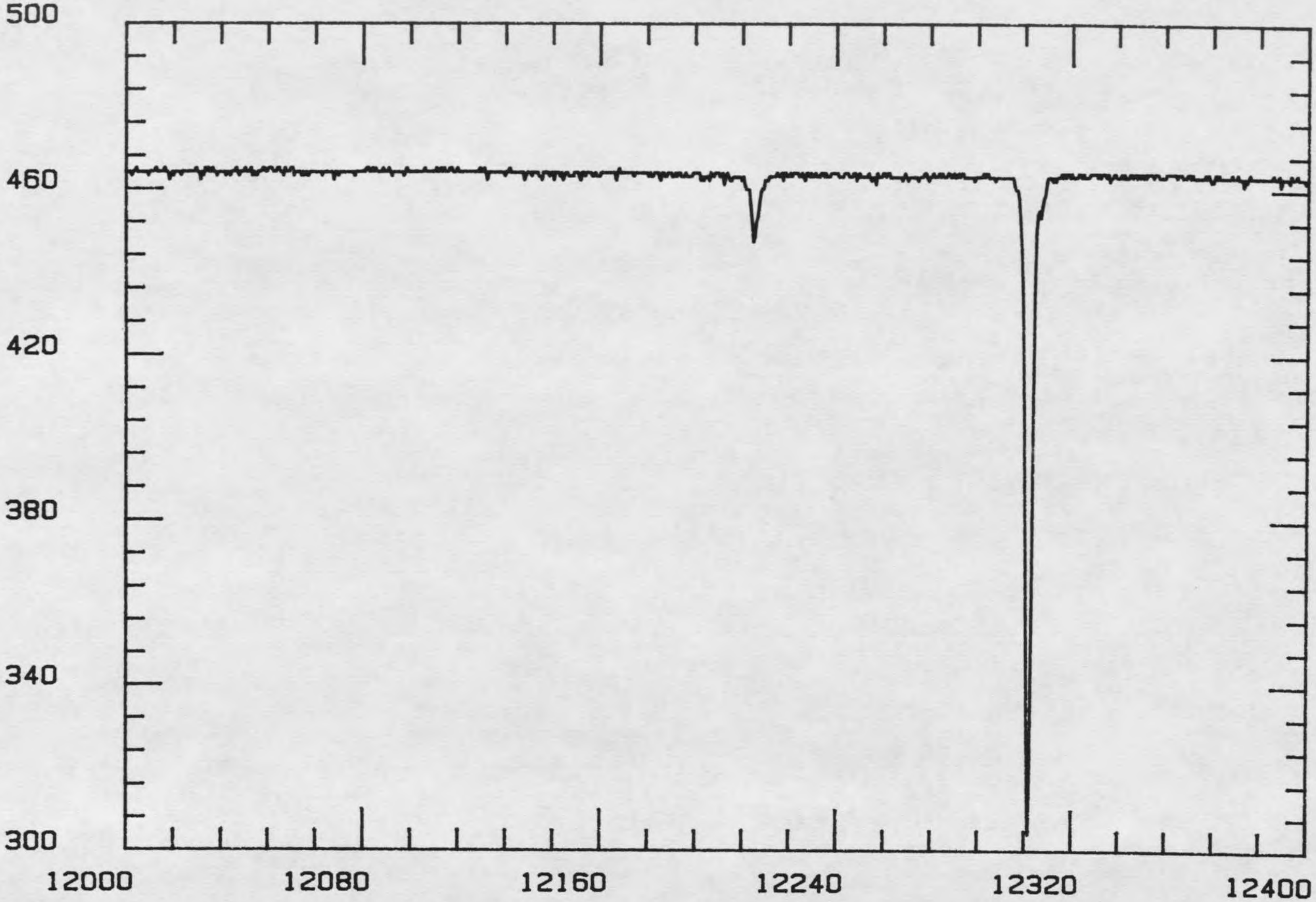

Figure 27. Fluorescence with no polarization at 12400.

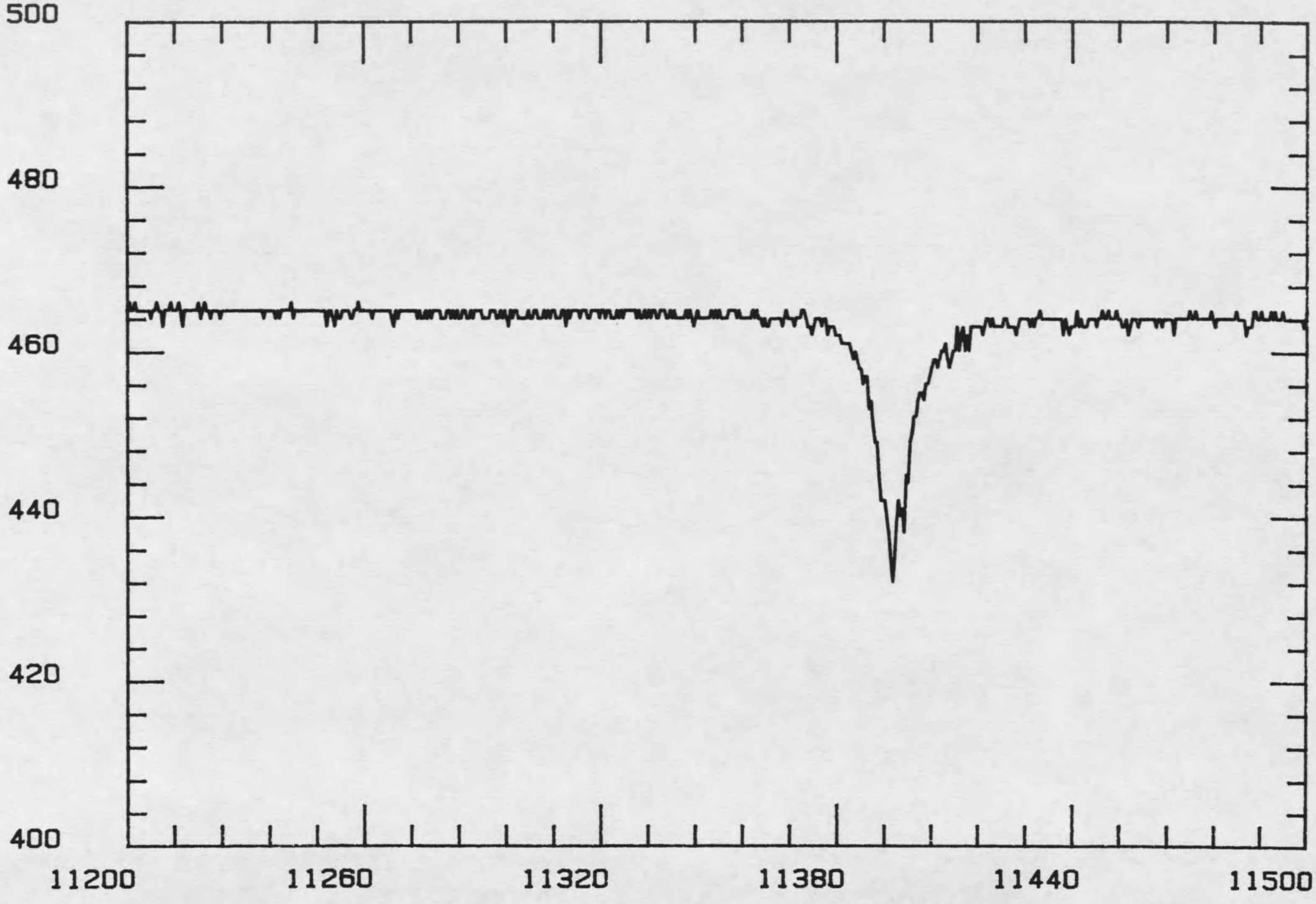

Figure 28. Fluorescence with no polarization at 11500.